คุณภาพด้านสีของกล้วยแผ่น

จากการทดลองพบว่าก ารเปลี่ยนสีของกล้วยแผ่นที่ได้หลังการอบแห้งด้วยลมร้อนอย่างเดียว และการอบแห้งด้วยลมร้อนร่วมกับการพัฟฟิงด้วยไอน้ำร้อนยวดยิ่งจะมีสีโดยรวมเป็นสีเหลืองปนน้ำตาล โดยบริเวณรอบจุดศูนย์กลางของกล้วยแผ่นจะมีสีน้ำตาลเข้มมากที่สุด เนื่องจากมีปริมาณน้ำตาลมากกว่าบริเวณอื่น ๆ โดยผลของอุณหภูมิ เวลาพัฟฟิง และความชื้นของกล้วยแผ่นก่อนการพัฟฟิงต่อการเปลี่ยนแปลงสีของกล้วยแผ่นในเทอมของ L, a และ b ดังแสดงในรูปที่ 2 ซึ่งจะประกอบด้วย surface plot และ contour plot

รูปที่ 2 (ก) แสดงผลของอุณหภูมิของไอน้ำร้อนยวดยิ่งและเวลาพัฟฟิงต่อการเปลี่ยนแปลงสีของกล้วยแผ่น พบว่าเวลาพัฟฟิงมีอิทธิพลต่อความสว่าง (ค่า L) มากกว่าอิทธิพลของอุณหภูมิไอน้ำร้อนยวดยิ่ง เมื่อเวลาพัฟฟิงมากขึ้นค่า L ลดลง เนื่องมาจากที่เวลาพัฟฟิงนานขึ้นทำให้เกิดปฏิกิริยาสีน้ำตาลเพิ่มขึ้น สำหรับอิทธิพลของอุณหภูมิไอน้ำร้อนยวดยิ่งนั้นพบว่าการเพิ่มอุณหภูมิในช่วงระหว่าง 160-170°C ค่า L มีค่าลดลงหลังจากนั้นค่า L มีแนวโน้มเพิ่มขึ้น ทั้งนี้เนื่องจากที่อุณหภูมิพัฟฟิงต่ำนั้นหลังสิ้นสุดกระบวนการพัฟฟิงความชื้นของกล้วยแผ่นยังเหลืออยู่มากทำให้การอบแห้งในขั้นตอนที่ 3 นั้น ใช้ระยะเวลานานขึ้น

รูปที่ 2 (ข) แสดงอิทธิพลของอุณหภูมิไอน้ำร้อนยวดยิ่งและเวลาพัฟฟิงต่อการเปลี่ยนแปลงค่า a ของกล้วยแผ่น พบว่าเมื่อเวลาพัฟฟิงนานและอุณหภูมิพัฟฟิงสูงขึ้น ค่าของ a ซึ่งแสดงความเป็นสีแดงมีค่าสูงขึ้น จากรูปจะเห็นว่า ที่เวลาพัฟฟิง 3 นาที เมื่ออุณหภูมิของการพัฟฟิงสูงขึ้น การเปลี่ยนแปลงของ a จะเป็นไปอย่างรวดเร็ว แต่ผลของอุณหภูมิอาจไม่เด่นชัดนักเมื่อเวลาในการพัฟฟิงสั้น (1 นาที) จากรูปค่า a มีค่าต่ำสุดเท่ากับ 6.12±0.7 ที่อุณหภูมิของไอน้ำร้อนยวดยิ่ง 180°C และ เวลาในการพัฟฟิง 1 นาที

รูปที่ 2 (ค) แสดงอิทธิพลของอุณหภูมิไอน้ำร้อนยวดยิ่งและวลาพัฟฟิงต่อการเปลี่ยนแปลงค่า b ของกล้วยแผ่น พบว่าเวลาพัฟฟิงจะมีอิทธิพลต่อค่า b มากกว่าอิทธิพลของอุณหภูมิไอน้ำร้อนยวดยิ่ง แต่อย่างไรก็ตามช่วงของค่า b ที่เปลี่ยนแปลงจะแคบมากโดยค่า b อยู่ระหว่าง 19.25 และ 20.29 ตลอดเงื่อนไขการทดลอง

การหดตัวของกล้วยแผ่น

รูปที่ 3 แสดงอิทธิพลของเวลาพัฟฟิงและอุณหภูมิของไอน้ำร้อนยวดยิ่งต่อร้อยละการหดตัวของกล้วยแผ่น พบว่า เมื่ออุณหภูมิของไอน้ำร้อนยวดยิ่ง และเวลาพัฟฟิงนานขึ้น ส่งผลให้ร้อยละการหดตัวของกล้วยแผ่นน้อยลง เนื่องจากที่อุณหภูมิสูงและเวลาพัฟฟิงนานขึ้นนั้นจะทำให้น้ำในกล้วยแผ่นเดือดกลายเป็นไออย่างรวดเร็ว เกิดความดันไอขึ้นภายในกล้วยแผ่น โครงสร้างมีการพองตัวขึ้น ในการพัฟฟิงที่อุณหภูมิสูง และเวลาพัฟฟิงนานนั้น ความชื้นของกล้วยแผ่นหลังกระบวนการพัฟฟิงจะเหลืออยู่น้อยมากทำให้โครงสร้างมีเสถียรภาพมากขึ้นเมื่อนำไปอบแห้งในขั้นตอนสุดท้ายโครงสร้างจะไม่มีการยุบตัวอีก ทำให้ร้อยละการหดตัวมีน้อย

คุณภาพด้านเนื้อสัมผัสของกล้วยแผ่น

คุณภาพด้านเนื้อสัมผัสของกล้วยแผ่น จะพิจารณาจากค่าความแข็ง จำนวนยอด และ ความชันเริ่มต้น โดยที่จำนวนยอดและความชันเริ่มต้น แสดงถึงความกรอบของผลิตภัณฑ์ หากจำนวนยอดและความชันเริ่มต้นมาก ก็แสดงว่าผลิตภัณฑ์มีความกรอบมาก เนื่องจากยอดเกิดจากการเปลี่ยนแปลงความชันของกราฟความสัมพันธ์ระหว่างแรงกับระยะทาง ซึ่งการเปลี่ยนแปลงความชันเกิดจากผลิตภัณฑ์มีช่องว่างหรือโพรงอากาศภาย

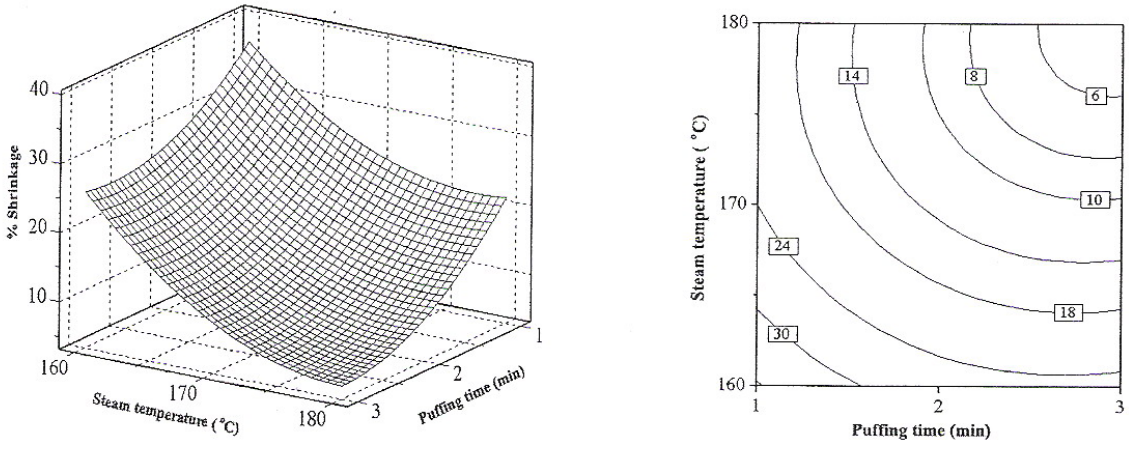

รูปที่ 3 ผลของอุณหภูมิและเวลาพัฟฟิงต่อการหดตัวของกล้วยแผ่น(ความชื้นของกล้วยแผ่นก่อนการพัฟฟิง 25% d.b.)

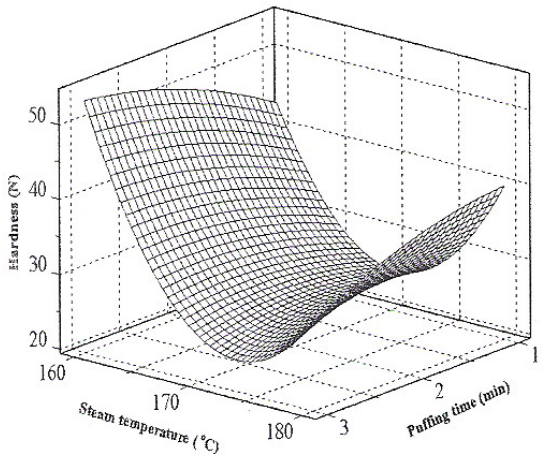

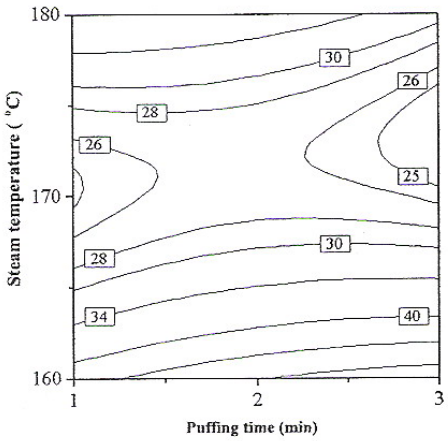

(ก) ผลของอุณหภูมิและเวลาพัฟฟิงต่อความแข็งของกล้วยแผ่น

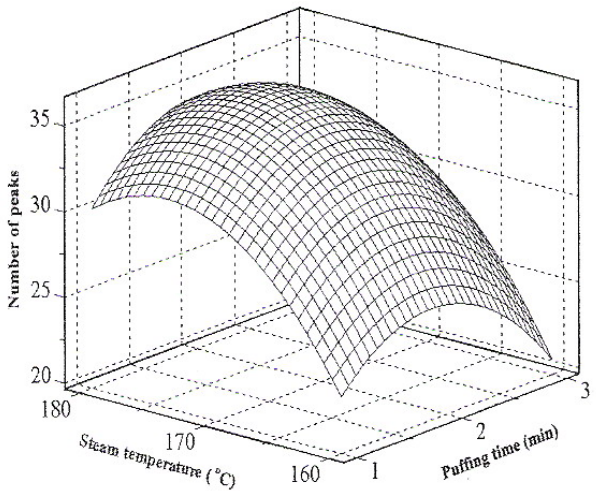

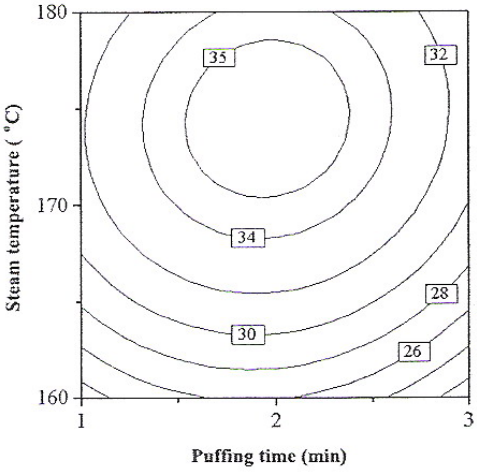

(ข) ผลของอุณหภูมิและเวลาพัฟฟิงต่อจำนวนยอดของกล้วยแผ่น

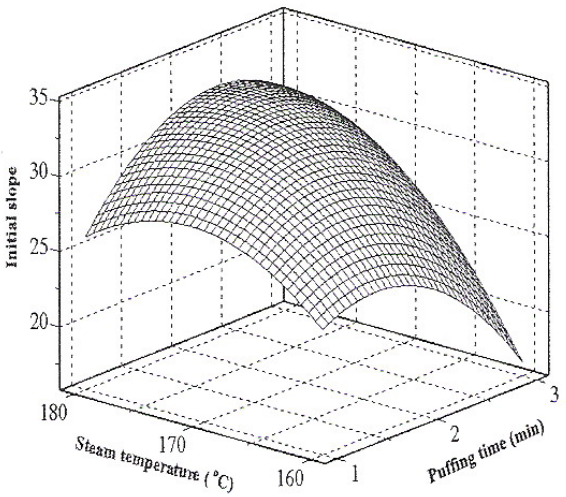

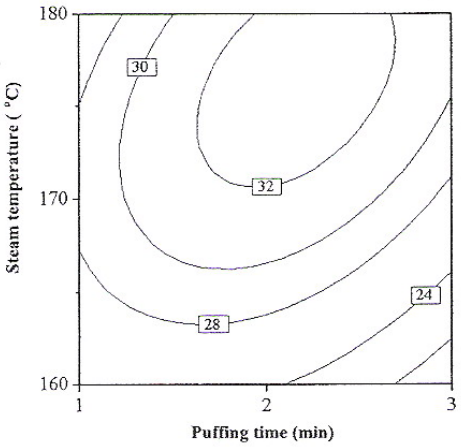

(ค) ผลของอุณหภูมิและเวลาพัฟฟิงต่อความชันเริ่มต้นของกล้วยแผ่น

รูปที่ 4 ผลของอุณหภูมิ และเวลาพัฟฟิงต่อเนื้อสัมผัสของกล้วยแผ่น (ความชื้นของกล้วยแผ่นก่อนการพัฟฟิง 25%d.b.)

ตารางที่ 4 ผลที่ได้จากการทำ optimization

	Hardness	Peaks	slope	Shrinkage	L-value	a-value	b-value
Optimal value	37.081	33.982	30.025	17.019	54.615	7.000	20.238
Individual Desirability (d_i)	0.996	0.999	1.000	0.999	0.9777	1.000	0.981
Composite Desirability (D)			0.994				

ใน ผลิตภัณฑ์ที่มีความกรอบมากจะมีจำนวนยอดมากและมีค่าความแข็งน้อย

รูปที่ 4 (ก) แสดงความสัมพันธ์ระหว่างอุณหภูมิของไอน้ำร้อนยวดยิ่งและเวลาพัฟฟิงต่อคุณภาพด้านความแข็งโดยพิจารณาที่ความชื้นของกล้วยแผ่นก่อนการพัฟฟิง 25 %d.b. พบว่าอุณหภูมิของไอน้ำร้อนยวดยิ่งมีผลต่อความแข็งของกล้วยแผ่นมากกว่าเวลาพัฟฟิง ซึ่งสังเกตได้จากความชันของเส้นกราฟ โดยที่พัฟฟิงด้วยไอน้ำร้อนยวดยิ่งที่อุณหภูมิต่ำกล้วยแผ่นจะมีความแข็งมาก เนื่องจากที่อุณหภูมิต่ำน้ำในวัสดุจะเดือดได้น้อย โครงสร้างเกิดการพองตัวได้น้อย ดังนั้นหลังกระบวนการพัฟฟิงกล้วยแผ่นเมื่อนำมาอบแห้งต่อทำให้ โครงสร้างที่ไม่มีเสถียรภาพจะยุบตัวลง (collapse) ซึ่งสอดคล้องกับข้อมูลของการหดตัวที่ได้กล่าวมาแล้ว โดยการหดตัวมากทำให้โครงสร้างมีรูพรุนน้อย มีความหนาแน่นมาก ทำให้กล้วยแผ่นมีความแข็งมาก

รูปที่ 4 (ข) และ (ค) แสดงความสัมพันธ์ระหว่างอุณหภูมิของไอน้ำร้อนยวดยิ่งและเวลาพัฟฟิงต่อจำนวนยอด และความชันเริ่มต้นของกล้วยแผ่นที่ความชื้นของกล้วยแผ่นก่อนการพัฟฟิง 25 %d.b. พบว่า อุณหภูมิไอน้ำร้อนยวดยิ่งมีอิทธิพลต่อจำนวนยอด และความชันเริ่มต้นของกล้วยแผ่นมากกว่าอิทธิพลของเวลาพัฟฟิง กล่าวคือเมื่ออุณหภูมิของไอน้ำร้อนยวดยิ่งสูงขึ้นจำนวนยอด และความชันเริ่มต้นมีค่ามากขึ้น เนื่องจากที่อุณหภูมิไอน้ำร้อนยวดยิ่งสูงนั้น น้ำภายในวัสดุจะเกิดการเดือด ทำให้เกิดความดันไอขึ้นภายในกล้วยแผ่นมาก กล้วยแผ่นจะเกิดการพองตัว โครงสร้างมีรูพรุนเกิดขึ้นมากทำให้กล้วยแผ่นกรอบมากขึ้น และที่เวลาพัฟฟิงมากขึ้นจำนวนยอดและความชันเริ่มต้นจะไม่เปลี่ยนแปลงมากนัก

การหาสภาวะที่เหมาะสมของการทดลอง

การหาจุดที่เหมาะสมของคุณภาพกล้วยอบกรอบ จะใช้ความพึงพอใจโดยรวม (Desirability Function) เพื่อหาค่าที่เหมาะสมของปัจจัยโดยการกำหนดค่า Weight function ของแต่ละผลตอบสนองด้านคุณภาพได้แก่ คุณภาพด้านสี และการหดตัว กำหนดค่า Weight เป็น 0.5 ด้วยเหตุผลที่ว่าในขั้นตอนการวัดสี และ การหาค่าการหดตัวของกล้วยแผ่นนั้นอาจมีความผิดพลาดอยู่บ้างทำให้ข้อมูลมีความแปรปรวนค่อนข้างมาก สำหรับคุณภาพด้านเนื้อสัมผัสกำหนดค่า Weight เป็น 0.1 ด้วยเหตุผลที่ว่าลักษณะการพองตัวของกล้วยแผ่นไม่สม่ำเสมอ ทำให้ข้อมูลที่ได้จากการวัดด้านเนื้อสัมผัสมีความแปรปรวนมาก และการกำหนด Importance ในงานวิจัยนี้จะให้ความสำคัญกับทุกผลตอบสนองเท่า ๆ กัน โดยค่า defaults ที่โปรแกรมกำหนดมาคือ 1

ตารางที่ 4 แสดงผลของคุณภาพกล้วยแผ่นที่ได้จากการทำ Optimization โดยสภาวะที่เหมาะสมสำหรับการพัฟฟิงกล้วยด้วยไอน้ำร้อนยวดยิ่งคือ อุณหภูมิของไอน้ำร้อนยวดยิ่งเท่ากับ 180 °C เวลาพัฟฟิงเท่ากับ 1.41 นาที และความชื้นก่อนการพัฟฟิงเท่ากับ 26.16%d.b.ที่สภาวะเงื่อนไขของกล้วยโดยความพึงพอใจโดยรวม (Composite Desirability) เท่ากับ 0.994

สรุปผล

จากการศึกษาปัจจัยต่าง ๆ ในกระบวนการพัฟฟิง คือ อุณหภูมิของไอน้ำร้อนยวดยิ่ง เวลาพัฟฟิง และความชื้นของกล้วยแผ่นก่อนการพัฟฟิงที่มีอิทธิพลต่อคุณภาพของกล้วยแผ่น พบว่า อุณหภูมิของไอน้ำร้อนยวดยิ่งมีอิทธิพลต่อคุณภาพของกล้วยแผ่นมากกว่าอิทธิพลของเวลาพัฟฟิง สำหรับความชื้นของกล้วยแผ่นก่อนการพัฟฟิงมีอิทธิพลต่อคุณภาพของกล้วยแผ่นน้อยมาก เมื่อพัฟฟิง กล้วยแผ่นที่อุณหภูมิสูงขึ้นและเวลาพัฟฟิงนานคุณภาพด้านสี ค่า a เพิ่มขึ้น และค่า L และ ค่า b ลดลง และเมื่อพัฟฟิงกล้วยแผ่นด้วยไอน้ำร้อนยวดยิ่งที่อุณหภูมิสูง(เวลาพัฟฟิงสั้น ๆ) ทำให้คุณภาพของกล้วยแผ่นด้าน การหดตัว และความแข็งลดลง แต่ความกรอบเพิ่มขึ้น และคุณภาพด้านสีค่าความเป็นสีแดง(ค่า a) ต่ำ สภาวะที่เหมาะสมของกระบวนการพัฟฟิงที่ให้ค่าการหดตัวน้อย ค่าความแข็งต่ำ มีความกรอบมาก และ สีดีที่สุด คือที่อุณหภูมิของไอน้ำร้อนยวดยิ่งเท่ากับ 180°C เวลาที่ใช้ในการพัฟฟิงเท่ากับ 1.4 นาที และ ความชื้นของกล้วยก่อนการพัฟฟิงเท่ากับ 26.16%d.b.

คำขอบคุณ

ผู้วิจัย ขอขอบคุณสำนักงานคณะกรรมการอุดมศึกษาและ

สำนักงานกองทุนสนับสนุนการวิจัย (สกว.) ที่ให้ทุนอุดหนุนการวิจัย และ ขอขอบคุณสำนักงานความร่วมมือเพื่อการพัฒนาระหว่างประเทศ (สพร.) ที่ให้ทุนสนับสนุนงานวิจัย

เอกสารอ้างอิง

เพลินใจ ตังคณะกุล. 2546. การทำข้าวเกรียบเป็นผลิตภัณฑ์คุณภาพ. อาหาร. 33(2): 90-93.

Demirel, D. and Turhan, M. (2003). Air-drying behavior of dawrf cavendish and Gros Michel banana slices. Journal of Food Engineering., 59(1), 1-11.

Hwang, M.P., & Hayakawa, K.I. (1980). Bulk densities of cookies undergoing commercial baking processes. Journal of Food Science., 45(5), 1400-1402.

Myers,R., & Montgomery,D.C. (2002). Response surface Methodology. New York, USA: Wiley.

Prachayawarakorn, S., Soponronarit, S., Wetchacama, S.and Jaisut, D. (2002). Desorption isotherms and drying characteristics of shrimp in superheated steam and hot air. Drying Technology., 20(3), 669-684.

Tang, Z. and Cenkowski, S. (2000). Dehydration dynamics of potatoes in superheated steam and hot air. Canadian Agricultural Engineering., 42(1), 6.1-6.13.

Proceedings of 5th International Conference On Innovations In Food and Bioprocess Technology, 7-9 December 2010

Effect of Osmotic Treatment and Puffing Temperature on Textural Properties of Banana Slices

S. Tabtiang[1] , S. Soponronnarit[1] and S. Prachayawarakon[2]

[1]Energy Technology Division, School of Energy Environment and Materials, King Mongkut's University of Technology Thonburi, Suksawat 48 Road, Tungkru, Bangkok 10140, Thailand, E-mail: ohmpare@hotmail.com

[2]Faculty of Engineering, King Mongkut's University of Technology Thonburi, Suksawat 48 Road, Tungkru, Bangkok 10140, Thailand, E-mail: somkiat.pra@kmutt.ac.th

[*]Corresponding author: somkiat.pra@kmutt.ac.th

Porous structure in food, a very important characteristic to crisp product, can be produced by intensive heating technique. However, the color of puffed product may have intense brown. To limit the brown reaction, the banana slice needed to be treated before puffing. This research was therefore to study on the effect of osmotic treatment on quality of puffed banana. The banana with 20-23°Brix total soluble solid was immersed into sucrose solution concentrations at 30, 35 and 40°Brix and dried at 90°C using hot air until the sample moisture content reduced to 30% dry basis (d.b.). After that, the banana slices were puffed by superheated steam at 180, 200 and 220°C for 150 s and dried again at 90°C until the sample moisture content reached 4% d.b. From the experimental results, it was found that the osmotic dehydration can improve the color of banana. The puffed osmotic banana was less brown than the puffed none osmotic banana as indicated by the L-, a- and b- values. The puffing temperature and osmotic concentrations did not enhance the browning rate. The osmotic dehydration limited the banana cell wall expansion, and resulted in the significantly larger shrinkage of osmotic sample than the none osmotic one. . In addition, the osmotic product had less porous as visually observed by scanning electron

microscope. Such morphology of osmotic banana directly affected the textural properties in terms of hardness, initial slope and number of peaks.

Keywords: Puffing, Banana, Drying, Osmotic dehydration, Texture, Color

Introduction

Bananas, one of the most popular fruits in tropical climate country, deteriorate rapidly after harvest. To reduce their losses, bananas are processed to various types of product such as fried banana, osmotic banana and puree banana. The fried banana is the one of those products which is more favourite because it attain crispy texture (Ali, 2008). However, the obtained product contains high oil content and can not be kept for an extended period of time due to possible lipid oxidation leading to rancidity. Thus, the free oil crisp banana is an alternative product. To obtain the crisp texture, the food material needs high porosity.

There are several drying techniques to produce high porous food material such as high temperature and short time drying (Saca and Lozano, 1992; Hofsetz *et al*., 2007; Varnalis *et al.*, 2001), microwave drying (Maskan 2000; Erle and Schubert, 2001) and low pressure superheated steam drying (Devahastin *et al.*, 2004; Elustondo *et al.*, 2001). In this work, the high temperature and short time drying technique was chosen.

During puffing process, some amounts of moisture or gas inside the food suddenly vaporize or expand. It can build up pressure and force the food structure to be expanded, thereby producing the porous structure of food products. The product characteristics after puffing has low bulk density (Kim and Toledo, 1987; Saca and Lozano, 1992). Moreover, the puffing process can save drying time (Sullivan *et al*, 1980; Saca and Lozano, 1992) and provide 40% energy saving as compared to the conventional hot air dehydration (Sullivan, *et al* , 1980).

The puffing medium normally uses the hot air since it is convenient in practice. For this research, the superheated steam will be used because the steam condensation at the material surface during the initial drying period can release the latent heat which results in the rapid rise in temperature of food material to stay at boiling point temperature of water. (Taechapairoj *et al*., 2003; Rordprapat *et al*., 2005) This may increase rapidly vapor pressure inside the product and thus provides a high expansion of product. However, the study of puffing with superheated steam has been limited in literature. Saca and Lozano, (1992) studied the puffing of banana using superheated steam at temperature of 152-

175°C and steam pressure at 0.8-2.8 kg/cm. It was found that the puffed banana had higher porosity than the conventional air dried product. Although, the product contained very porous structure, the product color was brown. Such browning in food is caused by the none enzymatic browning reaction and pigment degradation.

The way to improve the color of product can be done by osmotic pretreatment. Sucrose is frequency used as osmotic agent (Krokida *et al.*, 2000; Mandala *et al.*, 2005; Antonio *et al*., 2008). During osmotic dehydration, the natural solutes existing in food material such as reducing sugar, acid and minerals flow out from food (Islam and Flink, 1982; Shi and Xue, 2009; Sagar and Kumar, 2009) and they are replaced by osmotic agent. Marquez and Anon (1986) found that monosaccharide, glucose and fructose, had more influent on brown color development than sucrose.

Moreover, the sugar pretreatment before puffing process can improve shrinkage properties. Many researchers studied the effect of sugar on shrinkage properties of puffed products such as rice (Hsieh *et at*., 1990; Orts *et al*., 2000). They found that the osmotically puffed products had lower shrinkage or higher expansion volume than the none osmotically puffed products.
As mentioned-above, the objective of this work therefore was to study the effects osmotic solution concentrations and puffing conditions on the drying characteristics and quality of puffed banana. The quality parameter were considered in terms of color, shrinkage and textural properties.

2. Materials and methods

2.1 Material preparation

Fresh bananas were obtained from local market and their soluble solid contents were given in the range of 20-23°Brix. Before processing, the banana was sliced into 3.5 mm thickness and blanched by hot water at 95°C for 1 min.

2.2 Osmotic pretreatment

Osmotic solution was prepared by using commercial sucrose with concentrations of 30 35 and 40°Brix. The banana slices were immersed into various sucrose solution concentrations and the mass ratio of osmotic media to the sample was 30:1 to avoid the dilution effect. The samples were immersed into the osmotic solution until the moisture content of banana was not changed.

2.3 Puffing method

Puffing process used in this studies was consisted of 3 step; drying, puffing and drying. In the first step, the banana was dried by hot air at temperature of 90°C and air velocity of 2 m/s. When the moisture content reached to 30% d.b., the sample was puffed by superheated steam at temperatures of 180, 200 and 220°°C for 150 s. In the last drying stage, the banana was dried with hot air at the same temperature as the first stage drying. The final moisture content required at 4% d.b. At the end of each experiment, the moisture content of samples was determined by drying them in the oven at 103°C for 3 hr.

2.5 Textural property evaluation.

The puffed banana slices were kept in aluminium foil bag at room temperature for 3 day before texture test. The banana sample were measured by using the texture analyzer (Stable Micro System, TA. XT. Plus, UK) with a 5 N load cell. The samples were fractured with a cutting probe (HDP-BSK type) using blade speed of 2 mm/s. The probe move down to the banana sample with a speed of 2 mm/s. The maximum compressive force, the initial slope and the number of peaks (over 50 g force threshold) from force deformation curve were considered as an hardness, stiffness and crispness, respectively.

2.6 Color measurement

The color of dried samples were measured using a colorimeter (HunterLab, ColorFlex, UK). In each sample, the measurement were performed at different six positions and the measurement value was reported as the average value. The color were expressed as L-value (Brightness), a-value (redness/greenness) and b-value (yellowness/blueness).

2.6 Shrinkage determination

Ten samples were used to determine shrinkage. The volume of each sample was determined by the volumetric displacement method using n-heptane as the replacement medium (Saca and Lozano, 1992). The shrinkage was defined as the ratio of the dried sample volume to the original sample volume

$$\% \text{ shrinkage} = \frac{V}{V_i} \times 100$$

where V_i and V are the volume of the fresh sample and the volume of dried sample.

2.7 Glucose, fructose and sucrose determination

Determination of sugar content was performed according to AOAC method 982.14 with some modification. The sample of 5-10 g was pulverised and mixed with 50 mL water in a 100 mL volumetric flask. 1 mL 15% $K_4(Fe(CN_6))3H_2O$ and 1 mL 30% $ZnSO_4$ $7H_2O$ was added into the solution in order to extract

protein. After that, it was filtered through filter paper No. 42. The filtered solution from the last step was filtered through 0.45 μm nylon syringe filter. The final volume of solution kept at refrigerator until its chromatographic analysis. The 10 μL aliquots of the filtered solution were injected into HPLC.
The High Performanace Liquid Chromatography consist of a Prevail Carbohydrate ES column (4.6 mm, 25 cm; 5μm)(Alltech, Derfield, USA), a pump and a controller (Agilent, 1100, USA), autosampler (Agilent, 1100, USA) and a evaporative light scattering detector (ELSD detector) (Alltech , 500 ELSD, USA).

The fructose and glucose which are sugar isomers can clearly separate peaks by gradiant elution in column at 1 mL/min flow rate. The gradient elution was varied the portion of mobile phase. The mobile phase used contained acetonitrile and water. The column temperature was kept 30°C and the detector was carried out at drift tube temperature at 50°C and nitrogen flow rate 1.5 L/min. Peaks of samples were quantified with standard.

2.8 Statistical analysis
The experimental data of color, textural and shrinkage properties was analyzed by using an analysis of variance (ANOVA) and presented as mean value with standard deviations. Duncan's test was used to establish the multiple comparisons of the mean values. The mean values were considered significantly different when $p \leq 0.05$

Results and discussion

1. Effect of Osmotic Concentrations on Water loss and Solid Gain

Table 1 shows the moisture loss, solid gain and the losses of native sugars of banana slices immersed into sucrose solutions at 30, 35 and 40°Brix. The banana slices immersed into the higher sucrose concentrations lost the larger amounts of their moisture content. The possible explanation was related to the osmotic pressure difference between intracellular fluid in banana and osmotic solution. When the sample was immersed into the higher sucrose concentration, the osmotic pressure difference was higher, resulting in the larger loss of moisture content. At the same time, the solid gain increased, due to the diffusion of sucrose from the solution into the sample. As shown in Table 1, the solid gain increased from 24.8% to 32.6% when the osmotic concentration increased from 30°Brix to 40°Brix. From these results, the ratios of water loss to solid gain increased with the increased sucrose solution concentrations, implying loss of moisture content larger than the solid gain. This is because the size of sucrose

molecule is larger than that of water molecules. Hence, the water molecule can move with a rate faster than the sucrose molecule.

Table 1 also shows that the native sugars i.e. glucose and fructose disappeared during osmosis. The remaining amounts of glucose and fructose in the samples immersed into the sucrose solution concentrations were not rather different; the percent looses were 84-86% for glucose and 83-85% for fructose. From these results, it can be observed that the losses of glucose and fructose were nearly the same amount. This can be described by the fact that the glucose and fructose have the same molecular weight and this would be expected to have the same diffusion coefficient. Gekas *et al*. (1993) reported that the diffusion coefficients of glucose and fructose in water at 25°C were equal and had a value of 69×10^{-11} m^2/s.

Table 1 Immersion time, amount of water loss, amount of solid gain, moisture content, amount of sucrose, amount of fructose and amount of gluco of banana slice at various sucrose concentration.

Sucrose concentration (°Brix)	Immersion time (min)	Water loss (g water/ g dry mass)	Solid gain (g solid/ g dry mass)	Water loss/ Solid gain	Moisture content (% d.b.)	Amount of sucrose (g/100 g banana)	Amount of glucose (g/100 g banana)	Amount of fructose (g/100 g banana)
none osmotic					210.1 ± 3.5	7.43	1.04	1.12
30°Brix	240	0.321	0.248	1.29	134.1 ± 2.4	16.41	0.14	0.17
35°Brix	290	0.539	0.303	1.78	116.4 ± 3.7	18.45	0.16	0.19
40°Brix	330	0.772	0.326	2.37	102.4 ± 3.1	22.86	0.14	0.16

2. Shrinkage

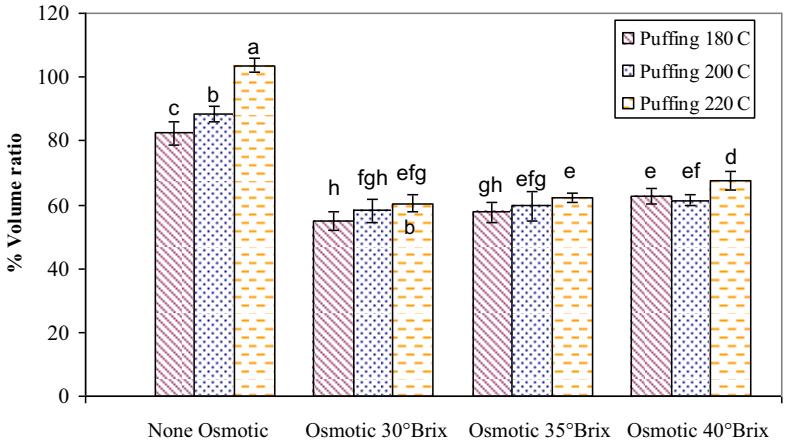

The different scripts presented over the bar mean the significant difference at $p \leq 0.05$.

Figure 1 Effects of puffing temperatures and osmotic solution concentrations on volume ratio.

Fig. 1 shows the shrinkages of none osmotic and osmotic samples both puffed at 180 200 and 220°C. The volume ratio of osmotic banana samples was significantly lower than that of the none osmotic ones for all puffing temperature. These results can be explained by the fact that the OH group of n-$C_6H_{12}O_6$ may bound with OH group in the cellulose of banana by hydrogen bonding (Allan *et al*, 2001). Consequently, the banana cell wall become stronger, allowing the small expansion of cellular structure during puffing and subsequently providing higher degree of banana shrinkage. The sucrose solution concentration affect on degree of banana shrinkage.

Considering the puffing temperature effect, it affected significantly the degree of shrinkage for both osmotic and none osmotic banana samples. The high puffing temperature provided lower degree of shrinkage. As showing in Fig 1, the volume ratio of none osmotic sample was 82% at puffing temperature of 180°C and increased to 103% at the puffing of 220°C.

Fig. 2 demonstrates morphologies of osmotic banana samples prepared from sucrose solution concentrations of 30, 35 and 40°Brix and puffed at temperature of 200°C. The morphologies of osmotic and non osmotic banana samples were noticeably different. The structure of osmotic banana samples was dense and exhibited less porous, but it was very porous for the none osmotic sample. As shown in Fig. 2 (a), the none osmotic banana had a huge pore with size larger than 1 mm. at the internal area of the sample. The formation of huge pore implies that there was a rapid vaporization of moisture inside the none osmotic samples during puffing, resulting in increasing vapor pressure inside the banana sample and the subsequent cell wall expansion. However, the cell wall expansion was occurred rarely in the osmotic banana samples. From their morphologies, it confirmed the shrinkage results, showing the higher shrinkage for the osmotic banana.

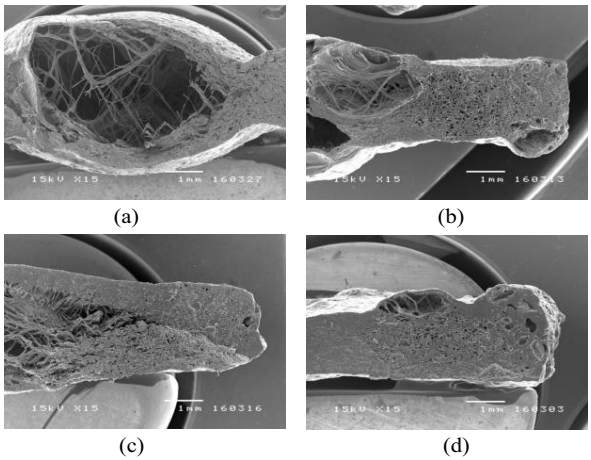

Figure 2 SEM photographs showing cross section of banana slices puffed at 200°C; (a) none osmotic; (b) 30°Brix; (c) 35°Brix; and (d) 40°Brix.

3. Texture

The force deformation curves represents the characteristics of crisp product. The product that was many fracture points indicate a crispy characteristic (Hofsetz and Lopes, 2005) and the number of jags on the force deformation curves indicate the porosity in samples. Fig. 3 shows the force deformation curve of osmotic and none osmotic samples at puffing temperatures of 180, 200 and 220°C. The force deformation curves of the osmotic samples were clearly different from those of the none osmotic ones. While the cutting probe was acted on the osmotic samples, the force reached the maximum point about 250-270 N. after which it was dropped sharply to zero, without any jag appearance. For the none osmotic samples, on the other hand, the force acting on the samples after reaching the maximum point did not drop rapidly to zero: it still appeared the several peaks. This can be explain by the fact that the sucrose solution causes banana tissue loosing the elasticity which in turn provides a sharp drop of force after the maximum point. This force characteristic indicated that the osmotic banana after puffing was brittle.

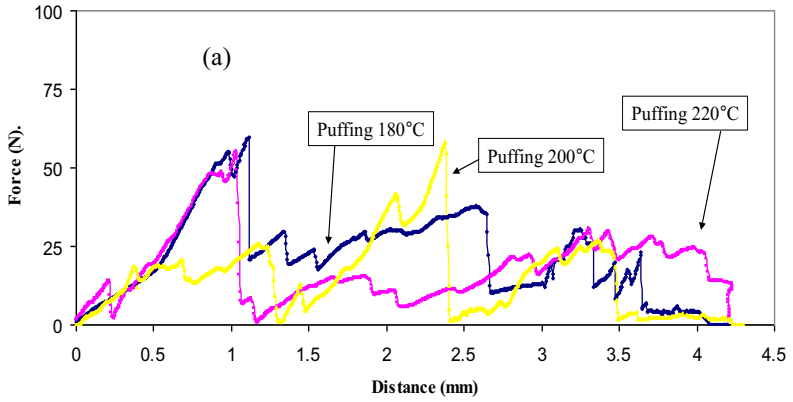

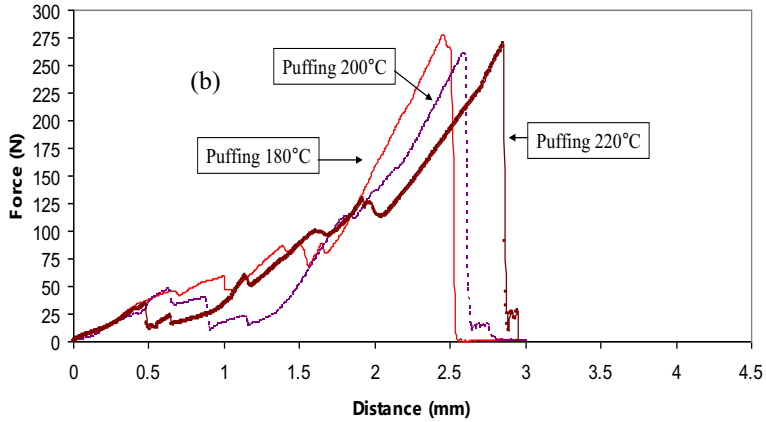

Figure 3 Force deformation curves: (a) the none osmotic banana and (b) the osmotic banana.

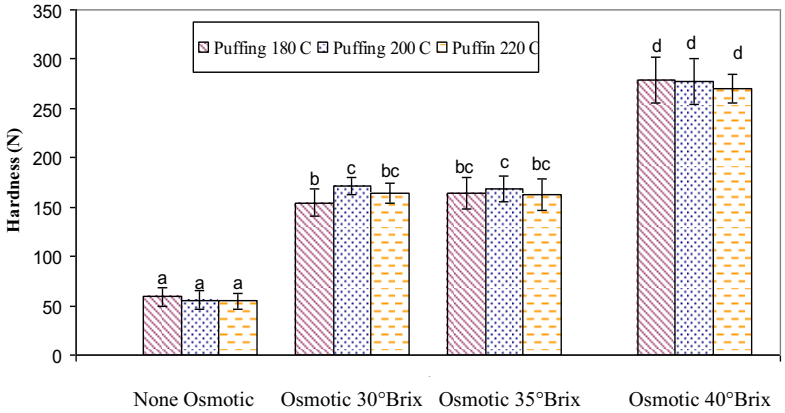

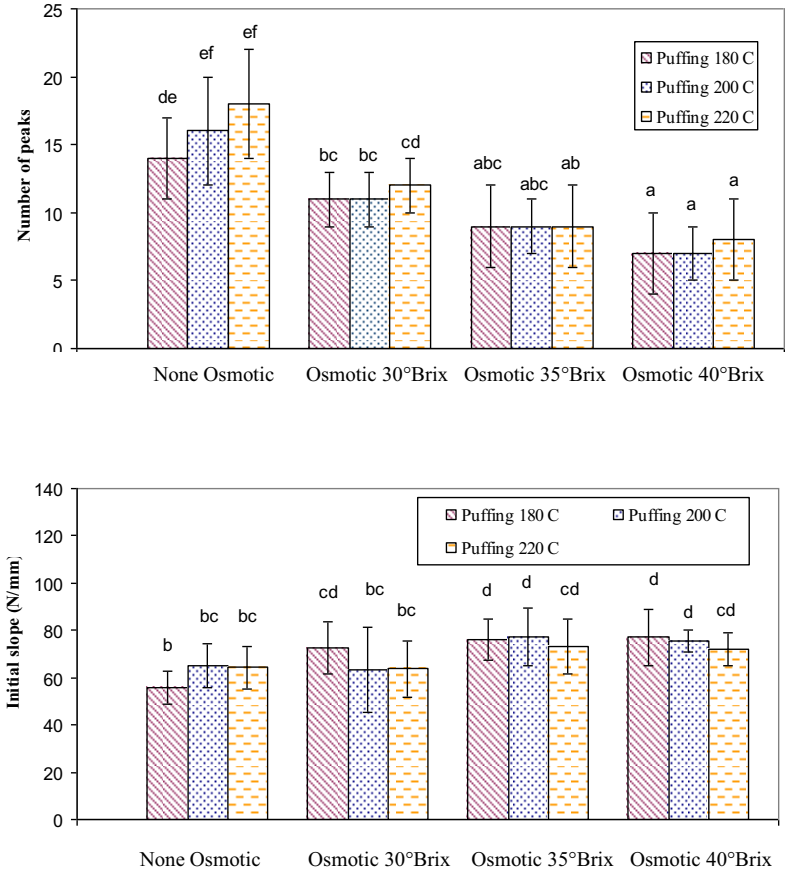

The different scripts presented over the bar mean the significant difference at $p \leq 0.05$.

Figure 4 Texture properties of the osmotic banana and the none osmotic banana.

Fig. 4 shows the effects of sucrose concentrations and puffing temperatures on the textural properties of none osmotic and osmotic banana samples. Considering at each sucrose solution, the puffing temperature given in a range of 180-220°C insignificantly affect the textural properties such as hardness, number of peaks and initial slope. The insignificant effect of puffing temperature on the textural characteristics for the none osmotic banana samples was also observed. On the other hand, the sucrose concentration strongly affected such textural

characteristics. Increase in both of hardness and initial slope and decrease in number of peaks were found with increasing in sucrose solution concentration.

As shown in Fig. 4, the banana slices pretreated with 40°Brix sucrose solution had the highest values for the of hardness initial slope but the smallest number of peaks. Such textural characteristics revealed that the osmotic banana product after puffing had a harder texture, less crispy and rather brittle than the osmotically untreated banana. The harder texture in the osmotic banana is related to the interaction between the OH groups of cellulose and sucrose solutions (Allan *et al*, 2001) which will improve the cellulose strength. These results corresponded to the morphological features as already mentioned.

4. Color

Table 2 shows the effect of the puffing temperatures and sucrose solution concentrations on the color of the bananas slices in terms of lightness (L), redness (a) and yellowness (b).

It was found that osmotic pretreatment can improve the color of banana samples compared with the color of samples without osmotic pretreatment. The color of osmotic samples had brownish-yellow but it had yellowish-brown for the banana without osmotic dehydration. It can indicated by the osmotic sample had higher of L- and b- values and lower of a-value than the none osmotic samples.

The color improvement of osmotic banana can be explain by the fact that the monosaccharide which is the main active component for none-enzymatic browning reaction (Pulis, 2010), leak out during the osmotic dehydration. Thus the browning rate is retarded and resulted in less brown for osmotic samples than the none osmotic sample. The osmotic concentration had not affect on the color of the osmotic samples indicated by L-, a- and b- values which shows insignificant difference among the samples at various sucrose concentrations.

Considering the effect of puffing temperature, it was found that the puffing temperature affect on the color of none osmotic samples. The color of none osmotic samples trend to intensive brown when the puffing temperature was increased as indicated by higher a value. In contrast, the puffing temperature did not affect on the product color of osmotic samples.

Table 2 color of dried osmotic banana slices and puffed none osmotic banana slices.

Drying Condition	L	a	b	Product color
Puffing 180°C	52.1^{ab} ±1.02	5.32^{cd} ± 0.3	16.81^{a} ± 0.83	
Puffing 200°C	51.3^{ab} ± 1.66	5.66^{cd} ± 0.25	16.85^{a} ± 0.85	
Puffing 220°C	49.5^{a} ± 1.5	6.11^{e} ± 0.21	16.3^{a} ± 0.83	
Puffing 180°C (30 °Brix)	59.29^{f} ±1.51	4.87^{abc} ±0.26	19.97^{cd} ±0.74	
Puffing 200°C (30 °Brix)	59.1^{ef} ± 2.73	4.93^{abc} ± 0.21	18.89^{bc} ± 1.11	
Puffing 220°C (30 °Brix)	57.22^{ef} ± 2.1	5.41^{cd} ± 0.33	18.68^{bc} ± 0.5	
Puffing 180°C (35 °Brix)	57.01^{ef} ±3.02	5.02^{abc} ± 0.32	16.65^{a} ± 0.9	
Puffing 200°C (35 °Brix)	58.35^{ef} ± 1.7	5.40^{cd} ± 0.51	18.15^{bc} ± 0.50	
Puffing 220°C (35 °Brix)	56.36^{de} ± 2.45	5.06^{abcd} ± 0.3	18.39^{bc} ± 0.54	
Puffing 180°C (40 °Brix)	57.43^{ef} ± 1.28	5.02^{abc} ± 0.28	18.68^{bc} ± 0.97	
Puffing 200°C (40 °Brix)	57.31^{ef} ± 1.3	5.2^{cd} ± 1.3	18.71^{bc} ± 0.83	
Puffing 220°C (40 °Brix)	54.19^{bcde} ± 4.22	5.27^{bcd} ± 0.32	17.7^{b} ± 1.14	

Different superscripts values are significantly different at 95% confidence level.

Conclusions

Osmotic pretreatment of banana slices can limit the browning reaction so the color of final osmotic product can improve. The color of osmotic product obtained at sucrose solution concentrations and puffing temperatures were not different. In spite of color in product, the osmotic pretreatment provided the texture of product to be harder and less crispy than the none osmotic banana. This is because the osmotic product had less porous as revealed by scanning electron microscope. The shrinkage was also high for the osmotic banana. Increase of sucrose solution concentration provided lesser extent of shrinkage whilst increase of puffing temperature did not affect on the textural properties of product.

Acknowledgements

The authors express their sincere thanks to Thailand Research Found, National Science and Technology Development Agency and King Mongkut's University of Technology Thonburi for supporting this financially project. Author Tabtiang thanks the Commission on Higher Education, Thailand for support the grant fund under the Strategic Scholarships for Frontier Research Network of the Ph.D. program Thai doctoral degree.

Reference

Ali, A. S. (2008). Banana chips [Online]. Available: www.practicalaction.org/practicalanswers/product: [5/10/2010].

Allan, G. G., Stoyanov, A. P., Ueda, M. and Yahiaoui, A. (2001). Sugar-cellulose composites V. The mechanism of fiber strengthening by cell wall incorporation of sugars. Cellulose **8**: 127-138.

Antonio, G. C., Alves, D. G., Azoubel, P.M., Murr, F. E. X. and Park, K. J. (2008). Influence of osmotic dehydration and high temperature short time processes on dried sweet potato (Ipomoea batatas Lam). Journal of Food Engineering **84**: 375-382.

AOAC (2006). Official method of analysis (18th ed.). Gaitherburg, Maryland: AOAC.

Devahastin, S., Suvarnakuta, P., Soponronnarit, S. and Mujumdar, A. S. (2004). A comparative study of low-pressure superheated steam and vacuum drying of a heat-sensitive material. Drying Technology **22**: 1845-1867.

Elustondo, D., Elustondo, M. P. and Urbicain, M. J. (2001). Mathermatical modeling of moisture evaporation from foodstuffs exposed to subatmospheric pressure superheated steam. Journal of Food Engineering **49**: 15-24.

Erle, U. and Schubert, H. (2001). Combine osmotic and microwave-vacuum dehydration of apples and strawberries. Journal of Food Engineering **49**: 193-199.

Gekas, V., Oste, R. and Lamberg, I. (1993). Diffusion in heated potato tissue. Journal of Food Science **58**: 827-831.

Hofsetz, K. and Lopes, C. C. (2005). Crispy banana obtained by the combination of a high temperature and short time drying stage and a drying process. Brazilian Journal of Chemical Engineering **22**: 285-292.

Hofsetz, K., Lopes, C. C., Hubinger, M. D., Mayor, L. and Sereno, A. M. (2007). Change in the physical properties of bananas on applying HTST pulse during air drying. Journal of Food Engineering **83**: 531-540.

Hsieh, F., Hu, L., Peng, I. C. and Huff, H. E. (1990). Pretreating dent corn grits for puffing in a rice cake machine. Journal of Food Science **55**: 1345-1355.

Islam, M. N. and Flink, J. M. (1982). Dehydration of potato II. Osmotic concentration and its effect on air drying behavior . Journal of Food Technology **17**: 387-403.

Kim, M. H. and Toledo, T. R. (1987). Effect of osmotic dehydration and high temperature fluidized bed drying on properties of dehydrated rabbiteye blueberries. Journal of Food Science **52**: 980-989.

Krokida, M. K., Karathanos, V. T. and Maroulis, Z. B. (2000). Effect of osmotic dehydration on color and sorption characteristics of apple and banana. Drying Technology **18**: 937-950.

Mandala, I. G., Anagnostaras, E. F. and Oikonomou, C. K.. (2005). Influence of osmotic dehydrations on apple air –drying kinetics and their quality characteristics. Journal of Food Engineering **69**: 307-316.

Marquez, G. and Anon, M. C. (1986). Influence of reducing sugars and amino acids in the color development of fried potatoes. Journal of Food Science **51**: 157-160.

Maskan, M. (2000). Microwave/air and microwave finish drying of banana. Journal of Food Engineering **44**: 71-78.

Orts, W. J., Glenn, G. M., Nobes, G. A. R., and Wood, D. F.(2000). Wheat starch effect on the textural characteristics of puffed brown rice cakes. Cereal Chemistry **77**: 18-23.

Purlis, E. (2010). Browning development in bakery product-A review. Journal of Food Engineering **99**: 239-249.

Rordprapat , W., Nathakaranakule, A., Tia, W. and Soponronnarit, S. (2005). Comparative study of fluidized bed paddy drying using hot air and superheated steam. Journal of Food Engineering **71**: 28-36.

Saca, A. S. and Lozano, E. J. (1992). Explosion puffing of bananas. International Journal of Food Science and Technology **27**: 419-426.

Sagar, V. R. and Kumar, P. S. (2009). Improvement of some process variables in mass transfer kinetics of osmotic dehydration of mango slices and storage stability. Journal of Scientific & Industrial Research **68**: 1043-1048.

Shi, J. and J. S. Xue (2009). Application and development of osmotic dehydration technology in food processing. In Advances in food dehydration; Ratti, C., Ed.; Taylor & Francis Group, LLC, New York, U.S.A.

Sullivan, J. F., Craig, J. C., Konstance, R. P., Egoville, M. J. and Aceto, N. C. (1980). Continuous explosion-puffing of apples. Journal of Food Science **45**: 1550-1558.

Taechapairoj, C., Dhuchakallaya, I., Soponronnarit, S., Wetchacama, S., Prachayawarakorn, S. (2003). Superheated steam fluidised bed paddy drying. Journal of Food Engineering **58**: 67-73.

Varnalis, A. I., Brennan, J. G. and MacDougall, D. B. (2001). A proposed mechanism of high-temperature puffing of potato. part I. the influence of blanching and drying conditions on the volume of puffed cubes. Journal of Food Engineering **48**: 361-367.

16th International Drying Symposium (IDS 2008)
Hyderabad, India 9-12 November 2008

DETERMINATION OF APPARENT DIFFUSIVITY OF MOISTURE IN PORES OF DRIED FOAM BANANA USING 2-D STOCHASTIC PORE NETWORKS

P. Prakotmak[1,*], S. Prachayawarakon[1], S. Soponronnarit[2]

[1,2] School of Energy, Environment and Materials, King Mongkut's University of Technology Thonburi, 126 Pracha-utit Rd., Bangmod, Thungkru, Bangkok, Thailand 10140 E-mail: preeda_list@hotmail.com, somkiat.pra@kmutt.ac.th*

[1] Department of Chemical Engineering, King Mongkut's University of Technology Thonburi, 126 Pracha-utit Rd., Bangmod, Thungkru, Bangkok, Thailand 10140

Abstract: Moisture diffusivity is an important parameter to predict the shelf life of food products. The main purpose of this research was therefore to determine the apparent diffusivity of moisture in pores of banana foam mat. 2-D stochastic pore network was used to represent the pore voids inside the banana foam sample and the moisture movements inside the individual pore segments were described by Fick's law. To obtain the moisture diffusivity, the experiments were carried out with standard static method using saturated salt solutions over a wide range of relative humidities and a temperature range of 35 to 45°C. Two banana foam densities of 0.3 and 0.5 g/cm^3, both having different porosities, were used to adsorb water vapor under the controlled condition. The interactions of transport processes within the pore network were illustrated using a 3-D pictorial representation of network concentration gradients in spaces with colour representing the moisture content. The network model could describe the experimental results relatively well. The diffusivity of water in pores was in order of 10^{-9} m^2/s which was 9 times higher than the apparent effective diffusivity. For a given temperature, the pore diffusivities were independent of the foam densities and relative humidity, except for the case of higher relative humidity of 70%. Moreover, the diffusivity depended strongly on the temperature.

Keywords: adsorption kinetics, banana foam mat, pore diffusivity, pore network

INTRODUCTION

Moisture migration during food storage is greatly important to many dry crispy products, such as biscuits, ready to eat cereals and snack foods, because the loss of their crispness strongly correlated to the moisture content. Rate of moisture adsorption in porous foods depends not only on the environmental conditions but also on their pore structures. Hence, understanding and capability to predict the moisture migration through their void spaces at different conditions are the main aspects that cannot be avoided in order to preserve their quality and to extend their shelf life as long as possible. To achieve this, model of porous food material is required and equation of moisture transfer is needed.

The moisture transport in porous foods can be mathematically by either a continuum or a discrete approach. In a continuum model, the porous spaces are considered as a continuum consistent with its appearance on macroscopic scale and effective macroscopic properties lump all the microscopic complexities of real pore network, including mechanisms of mass transfer which may be occurred by molecular diffusion and capillary flow etc. For adsorption under isothermal condition, moisture adsorption occurring in an infinite slab geometry can be described by

$$\frac{\partial M}{\partial t} = \nabla\left(D_{eff}\nabla M\right) \qquad (1)$$

By using eq.(1), the effective diffusivity, D_{eff}, can simply be determined from the adsorption experiments. The effective diffusivity can be expressed as

$$D_{eff} = \frac{\varepsilon D_A}{\tau} \qquad (2)$$

Tortuosity factor, τ, accounts for the fact that the pore spaces do not provide straight line paths through the particle, thereby lengthening the diffusive path and reducing the internal diffusional fluxes. At the present, however, there is no reference of the actual

diffusivity of water in pore voids, D_A. To estimate the water diffusivity in the pores, the model must include the information details about the interactions between internal diffusional fluxes and pores, which determine the pathways of moisture movement. The diffusivity of water can be estimated by first constructing the discrete network models, where more or less simplified geometry and pore size distribution are used to describe topology of pore structure of real material (Mann, 1993; Hollewand and Gladden, 1992; Androutsopoulos and Mann, 1979). Diffusion equation is then applied to individual pores of these simulated structures and the flow of substances through pore segments can be numerically predicted (Blunt, 2001; Yiotis et al, 2005; Prachayawarakorn, Prakotmak and Soponronnarit, 2008).

Network models represent the void spaces of a porous medium by a simple two-or more realistic three-dimensional lattice in which the large and small pores are randomly interconnected. Each pore can be assumed to be cylindrical, slit, triangular and polygonal shapes. Segura and Toledo (2005) found that pore shapes used in the network model had an insignificant effect on the drying characteristic curves, vapor relative diffusivity and liquid relative permeability.

As mentioned above, diffusivity data of water in the pores of the porous foods have not been available in the literature. The aim of the present investigation was therefore to determine the pore diffusivity by using a two dimensional stochastic pore network. The banana foam mat was used as a representative porous medium. The Fick's second law was used to describe the moisture diffusion in individual pore segments and an optimization technique was implemented to determine the pore diffusivity under adsorption conditions.

DRIED BANANA FOAM PREPARATION

The banana puree with 5% of fresh egg albumen used as foaming agent was foamed to densities of 0.3 and 0.5 g/cm^3. The banana foams was poured slowly into a steel block with a dimension of $43 \times 43 \times 4$ mm and then placed on a mesh tray, which was covered with aluminium foil. After that, it was dried to about 3% dry basis (d.b.) using 80^{o}C and a 0.5 m/s superficial air velocity. The sample thicknesses after drying were 2.8mm and 3.2mm for the banana foam densities of 0.3 and 0.5 g/cm^3, respectively.

ADSORPTION EXPERIMENT

Moisture adsorption experiments were carried out using the static method. Samples were placed into the glass jars contained the saturated salt solutions which ($MgCl_2$ 6·H_2O, $Mg(NO_3)_2$ 6·H_2O, KI, NaCl and KCl) give the relative humidity (RH) in range of 32-82% for the temperatures of 35, 40 and 45^{o}C. The glass jars were kept in the hot air oven with an accuracy of ±1°C (UFE500, Memmert, Germany). Samples were weighed at different exposure times until the moisture content of samples did not change. At high relative humidity (RH > 74%), a small amount of toluene was added into a small tube which was fixed in the glass jars in order to prevent microbial spoilage of the samples (Kaya and Kahyaoglu, 2005). Moisture content of each sample after reaching the equilibrium condition was determined by drying it with an oven at a temperature of 103°C for 3 h. The experiment at each sorption condition was repeated three times and the mean value was reported.

SEM PHOTOGRAPH

The morphologies of dried banana foam mats were characterized using scanning electron microscope (SEM) with an accelerating voltage of 10 kV. Before photographing, the specimens were cut into a dimension of 5×5 mm and then glued on the metal stub. The samples were coated with gold, scanned, and photographed at $15 \times$ magnification.

To quantify the porous banana foam characteristics such as pore diameter and pore area, Image J software was used. Each pixel of the SEM micrograph was assigned a value of gray intensity between 0 and 255 and the binary images were generated. The pixels with gray levels lower than the selected threshold were assigned as pore, which appeared as black colour, and the pixels with gray levels above the selected threshold were set as solid phase, which appeared as white colour in binary image. The pore diameter was estimated by the known pore area by assuming a spherical shape.

PORE NETWORK MODEL

When the pore size distribution of material is known, these pores are assigned according to their distribution and allocated randomly onto a lattice. In this work, the pore was assumed to be cylindrical geometry and each pore in the network had the same length. The pores with different sizes were randomly placed onto the network and this approach provided pore at any positions within the network independent to the neighbouring pores. Such random arrangement of pore assemblies was referred to as stochastic pore network. Figure 1 shows an illustrative 2-D stochastic pore network with a size of 23×50 consisting of 2373 pores obeying a pore size distribution of dried banana foam shown in Figure 6 for the initial density of 0.3 g/cm^3, but in calculating the pore diffusivity, we used a larger network size. In this work, we considered the 2-D parallelogram pore networks with a size of 20×231 consisting of 9491 pores for the sample at the initial foam density of 0.3 g/cm^3 and a size of 23×264 consisting of 12431

pores for the density of 0.5 g/cm^3. The distance between two pore bodies (L) was equal to 128 μm .

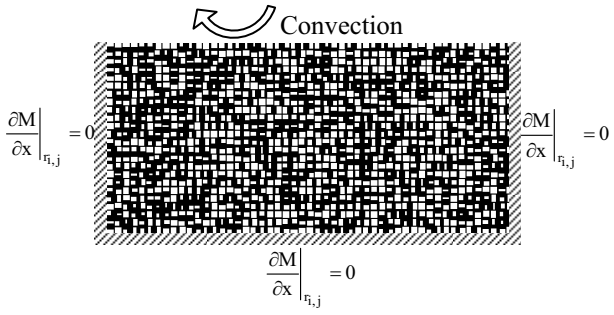

Fig. 1. Illustration of a simple 2-D stochastic pore network and boundary conditions.

Single Pore

In this work, moisture adsorption between surrounding air and banana foam mat occurred under isothermal condition. The moisture moved along the pore axis and it can be described by Fick's second law for the individual pores in the network:

$$\frac{\partial M}{\partial t} = D_p\left(\frac{\partial^2 M}{\partial x^2}\right) \qquad (3)$$

The migration of moisture from the surrounding air to the banana foam surface occurred specifically at the top surface and no moisture transferred at the bottom surface of the network since the banana foam mat was placed on an opaque glass dish. The samples had the length and width about 11 times of its thickness and thus, the banana foam mats were reasonably assumed to be an infinite slab. Accordingly, moisture movement during adsorption occurred along the material thickness direction. The constant diffusion coefficient at a given condition was assumed and the moisture profile in the pores at the beginning was uniform along the pore axis,

$$M = M_i \quad : t = 0, 0 \le x \le L \qquad (4)$$

The length of each pore, L, was calculated by dividing width of material by NV+1 where NV is the number of pores in each row of the network; 264 for the network size of 23×264 and 231 for the network size of 20×231 were used. Because the surface area at each sample side was remarkably smaller than that at the top surface, the moisture transferring from the surrounding to the pores allocated at the two sides of sample was small. Hence, the boundary condition for the pores allocated at both sides of the network is set as

$$\frac{\partial M}{\partial x} = 0 \quad : t > 0 \qquad (5)$$

For the periphery pores allocated on the top of the network, the moisture moving from the surrounding to those pores was occurred by convection and the boundary condition is set as

$$D_p\left(\frac{\partial M}{\partial x}\right) = h_m\left(M_e - M_s\right) \quad : t > 0 \qquad (6)$$

To calculate the moisture concentration of the pores, a finite difference method was used. An individual pore in the network was divided into n intervals (N=12) and Eq. (3) was discretized using the explicit method as follows:

$$M^{p+1}_{n,r_{i,j}} + M^{p}_{n,r_{i,j}}(2\alpha - 1) - \alpha\left(M^{p}_{n+1,r_{i,j}} + M^{p}_{n-1,r_{i,j}}\right) = 0 \qquad (7)$$

where $\alpha = D_p \Delta t / \Delta x^2$ is the Fourier number, p and n the respective indexes of the present time and of nodal position along the pore axis. The boundary conditions in Eqs. (5) and (6) can be written as:

$$M^{p+1}_{n,r_{i,j}} + M^{p}_{n,r_{i,j}}(2\alpha - 1) - 2\alpha\left(M^{p}_{n+1,r_{i,j}}\right) = 0 \qquad (8)$$

$$M^{p+1}_{n,r_{i,j}}(\gamma + 1) - M^{p+1}_{n-1,r_{i,j}} - \gamma M^{p+1}_{e} = 0 \qquad (9)$$

where $\gamma = h_m \Delta x / D_p$. The moisture adsorption rate $Q_{i,j}$ for the pore with radius of $r_{i,j}$, can be calculated by

$$Q_{r_{i,j}} = \pi r^2_{i,j} D_p\left(\frac{dM_{r_{i,j}}(x,t)}{dx}\right)_{x=L} \qquad (10)$$

Mass balance in the network

To determine the moisture contents at the pore junctions, the mass balance of moisture content at the inner nodes of network was made, assuming no accumulation at the pore junctions within the network, which is thus expressed by

$$\sum_{j \in \{i\}} Q_{r_{i,j}} = 0 \qquad (11)$$

where {i} refers to the set of i-adjacent nodes which are connected to node (i) in the network. After the moisture contents at every nodes of the network were known, the average moisture content $\overline{M}_{network}$ of network can then be calculated using the following equation

$$\overline{M}(t)_{network} = \frac{\sum_{n=1}^{Z} r^2_{i,j} \int_0^L M_{r_{i,j}}(x,t)dx}{Z \cdot L \sum_{n=1}^{Z} r^2_{i,j}} \qquad (12)$$

To estimate the apparent pore diffusion, D_p, the optimization technique using a golden-search method was used. The root mean square error (RMSE) for the residuals of the measured and predicted values of average moisture content was set as the objective

function with a tolerance of 10^{-5}. The RMSE is defined as

$$RMSE = \left[\frac{1}{K} \sum_{n=1}^{K} (M(t)_{exp} - \overline{M}(t)_{network})^2 \right]^{1/2} \quad (13)$$

where $M(t)_{exp}$ is the experimental moisture content of material at time t, $\overline{M}(t)_{network}$ is the predicted moisture content, and K is the number of the experimental data. The lower the value of RMSE is the better the goodness of fit. All computations were implemented using Intel C++ Compiler (http://www.intel.com) to run on a PC compatible with 3.0 GHz dual-processor and 2 GB of RAM.

RESULT AND DISCUSSION

Effect of temperature and relative humidity

Generally, if the partial vapor pressure or vapor concentration is greater in the surrounding atmosphere than in the porous materials, the moisture is then transferred from the air to the materials. The adsorption rate is extremely rapid when there is a great vapor pressure difference between the water in the air and the water in the adsorbent. The process of adsorption continues until the adsorbed layer is in thermodynamical equilibrium with gas or vapour.

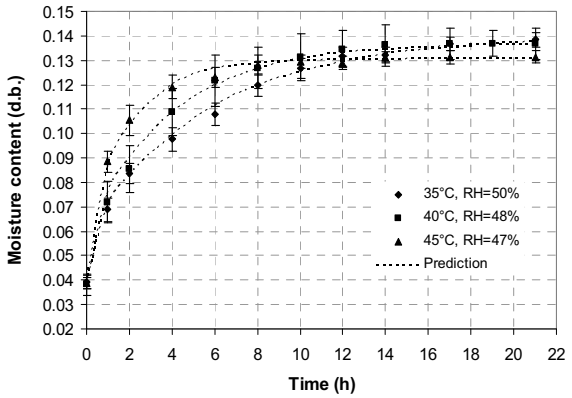

Fig. 2. Kinetics data of moisture adsorption at different temperatures and relative humidities for the initial banana foam density of 0.3 g/cm^3

The effect of partial vapour pressure on the adsorption rate can be studied by changing the temperature or relative humidity and the experimental results are shown in Figure 2 for the temperature effect and Figure 3 for the relative humidity effect.

As shown in Figure 2, the rate of moisture uptake was very fast during the early period of time and gradually decreased as the moisture content approached the moisture equilibrium. The higher adsorption rate was evident in elevated temperature and relative humidity. From the preliminary test, the banana foam mat lost its textures at the moisture content of 0.07 d.b. From this result, it indicated that the banana foam will lost the crispiness when it exposed to air about 40 minutes under the operating conditions at the relative humidity and temperature lower than 75% and 40°C, respectively.

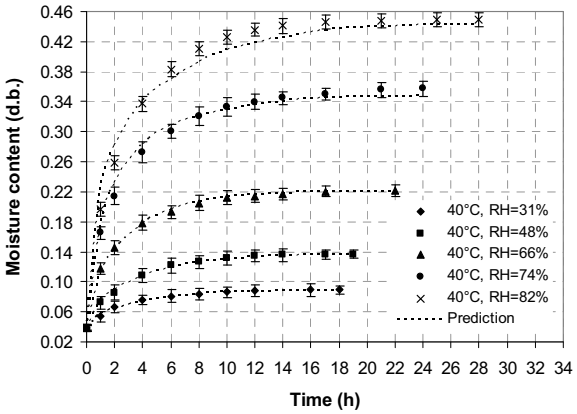

Fig. 3. Kinetics data of moisture adsorption at 40^{o}C and relative humidities of 31, 48, 66, 74 and 82% for the initial banana foam density of 0.3 g/cm^3

At the equilibrium state, the equilibrium moisture content tended to decrease with increasing temperature; these values were 0.1384, 0.1368 and 0.1308 d.b. for the temperatures of 35, 40 and 45^{o}C, respectively. This may attribute to the excitation states of water molecules. At elevated temperature, the molecules are in higher states of excitation, thus increasing their distance apart and, in turn, decreasing the attractive forces between them (Jamali et al., 2006). Similarly, Kim et al. (1999) and Palou et al. (1997) found that the sorption capacity or equilibrium moisture content of crackers and cookies decreased with increasing temperature.

Effect of initial foam density

Figure 4 shows the moisture adsorption kinetics at temperature of 45°C for the initial foam densities of 0.3 and 0.5 g/cm^3. It can be seen that the initial foam density strongly affects the moisture adsorption rate; the lower the initial foam density, the faster the adsorption rate. This is because the porosities of both banana foams were different; the void area fractions for the banana foam densities of 0.3 and 0.5 g/cm^3 were 31 and 26 %, respectively.

High porosity in porous foods provides less diffusional flux resistance and thus greatly facilitates the moisture transport to those porous foods. In the porous banana foam studied, the higher void area fraction for the banana foam density of 0.3 g/cm^3 is a result of the assembly of the giant pores with sizes larger than 150 μm which had a larger number (38%) than that at the foam density of 0.5 g/cm^3 as will be seen in Figure 6. These huge pores, serving as a massive transport of moisture through the interior pores, may be interconnected into almost all parts of the whole network. Hence, the rapid adsorption is

obviously evident for the foam density of 0.3 g/cm^3. Prachayawarakorn, Prakotmak and Soponronnarit (2008), who studied the effect of pore assembly architecture on the drying rate, found that full set of pores which were assembled in a different way exhibited different drying rates. As the network archetype with the large pore assembly allocated onto the network exterior and the smaller pores to the interior, the drying rate is very fast as compared to the other pore architectures.

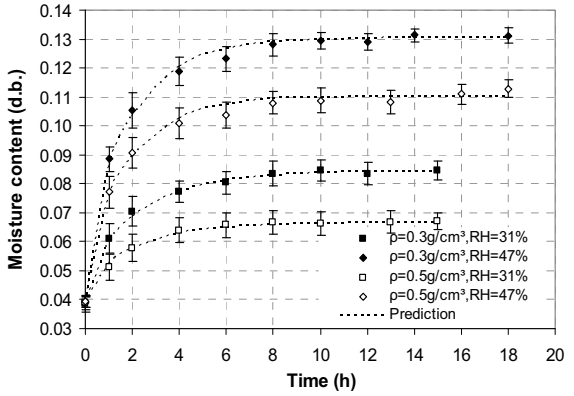

Fig. 4. Moisture adsorption kinetics at 45°C and relative humidities of 31 and 47% for the initial banana foam densities of 0.3 and 0.5 g/cm^3

As shown in Figure 4, the uptakes of moisture content into the banana foams after the elapsed time of 10 hours are very slightly and this indicated the system reaching the equilibrium state. At the equilibrium, the moisture content of banana foam at density of 0.3 g/cm^3 was apparently higher than that at 0.5 gm/cm^3 due to different porosities.

Pore size distribution

The microstructures of dried banana foam mats characterized by SEM are shown in Figures 5a and 5b for various initial foam densities. The corresponding binary images are illustrated in Figures 5b and 5d. The reconstructed porous structures of the banana foams in binary image reasonably represented their original images. As shown in Figures 5a and 5c, the pores were random in sizes and irregular in shape. Moreover, the porosity appears to form a mass of interconnecting pores in the banana foam sample. This would be clear that it is very task to understand the interactions between pore structure and diffusional fluxes of moisture by using a simple mathematical model.

Figure 6 shows the pore size distributions of the dried banana foams at the densities of 0.3 and 0.5 g/cm^3, both distributions obtained from the reconstructed pore structures. The characteristic of distributive pore sizes was reasonably described by grammar distribution. The sample with an initial foam density of 0.3 g/cm^3 had small pore assembly in the range 6 to 150 μm accounting for 62% of the whole number of pores and for 38% with the pores larger than 150 μm. For the density of 0.5 g/cm^3, it appears the proportion of small pores accounting for 71% which was higher than the sample at the density of 0.3 g/cm^3 for the same pore size range. However, the porosity of sample at the density of 0.5 g/cm^3 was relatively smaller as mentioned before because the large pores had a smaller number.

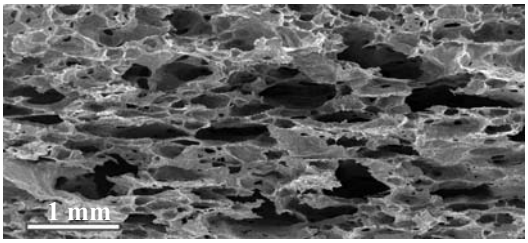

(a) 0.3 g/cm^3

(b) 0.3 g/cm^3

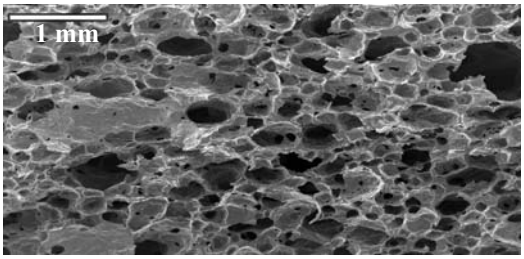

(c) 0.5 g/cm^3

(d) 0.5 g/cm^3

Fig. 5. (a,c) SEM micrographs of dried banana foam mats at different initial foam densities and binary images (b,d)

Apparent pore diffusivity

Figure 7 shows the values of pore diffusivity in banana foam at different temperatures and relative humidities. Considering at a given temperature, for example at 40°C, most moisture diffusivity data had a slight change for the humidity range below 70%, corresponding to the lower equilibrium moisture

contents than 0.2214 d.b. for all adsorption conditions used in this study. These results, when analyzed statistically with Duncan's test, showed an insignificant difference. The mean values of apparent pore diffusivity were in the order of 10^{-9} m^2/s. In fact, the orders of magnitude of the diffusion coefficients depend on the state of substance: for gases, approximately 10^{-5}; for liquids, approximately 10^{-9} (Aguilera and Stanley, 1999). From this information, it might be indicated that the transport of moisture through the banana foam mat mainly occurred in form of liquid. Similarly, Roca et al. (2006) reported that the adsorption of water vapor by sponge cake occurred mainly in liquid phase.

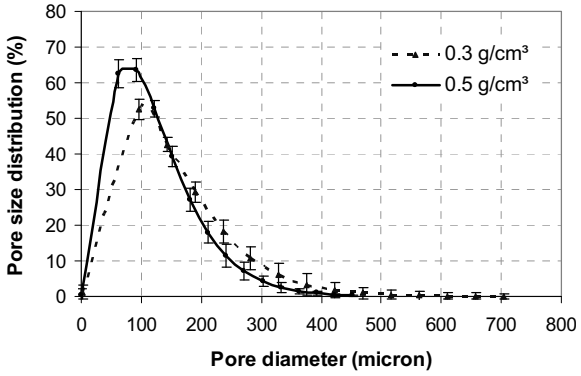

Fig. 6. Pore size distributions of dried banana foam at different densities

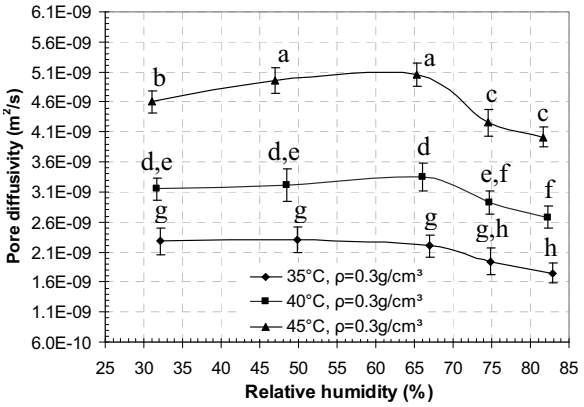

Fig. 7. Effects of temperatures and relative humidities on the pore diffusivities for the initial banana foam density of 0.3 g/cm^3: the same letter means insignificant difference (P>0.05)

Once the relative humidity was higher than 70% however, the pore diffusivity decreased relatively with increase in the relative humidity. In this case, the water vapor adsorption rate was very fast and the texture of banana foam was subsequently very soften as observed from the experiments, which leads to collapse of the pores and decrease of diffusivity as a consequent result. Figure 7 also presents the effect temperature on apparent pore diffusivity. As expected, the apparent pore diffusivity significantly increased with increase in temperature (P<0.05).

Figure 8 shows the apparent pore diffusivity of water for the samples at the initial foam densities of 0.3 and 0.5 g/cm^3. The pore diffusivity was slightly lower at the foam density of 0.5 g/cm^3 than at the density of 0.3 g/cm^3 for all experimental conditions. However, the statistical analysis of these pore diffusivity data showed the insignificant difference among the two initial foam densities.

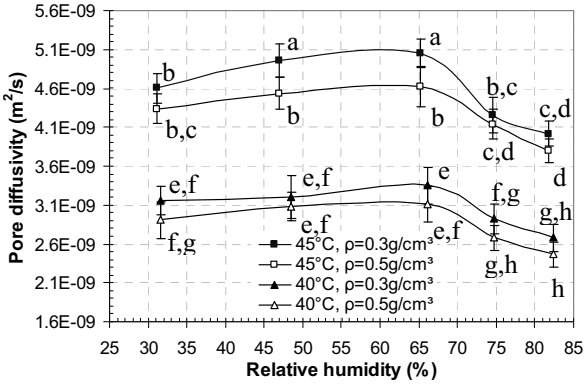

Fig. 8. Effect of initial foam densities on the apparent pore diffusivities at different relative humidities and temperatures of 40 and 45^{o}C: the same letter means insignificant difference (P>0.05)

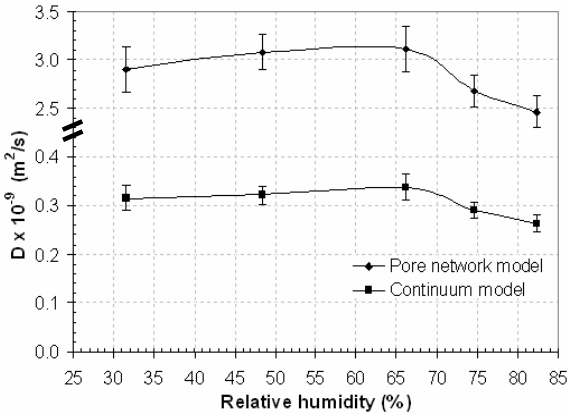

Fig. 9. Comparison between pore diffusivities and effective diffusivities of banana foam mat at 40 ^{o}C and relative humidities for the initial banana foam density of 0.5 g/cm^3

Figure 9 shows the comparison of the apparent pore diffusivity and the effective diffusivity. The value effective diffusivity was determined using Eq. (1) assuming that the moisture migration occurred in one dimension and the water vapour transported from the air to the top surface by convection. It can be seen that the effective diffusivity is approximately 9 times lower than the pore diffusivity. If the fraction void area for the banana foam density of 0.5 g/cm^3 was 0.26 as previously mentioned, the tortuosity factor calculated by Eq. (2) was 2.3.

.

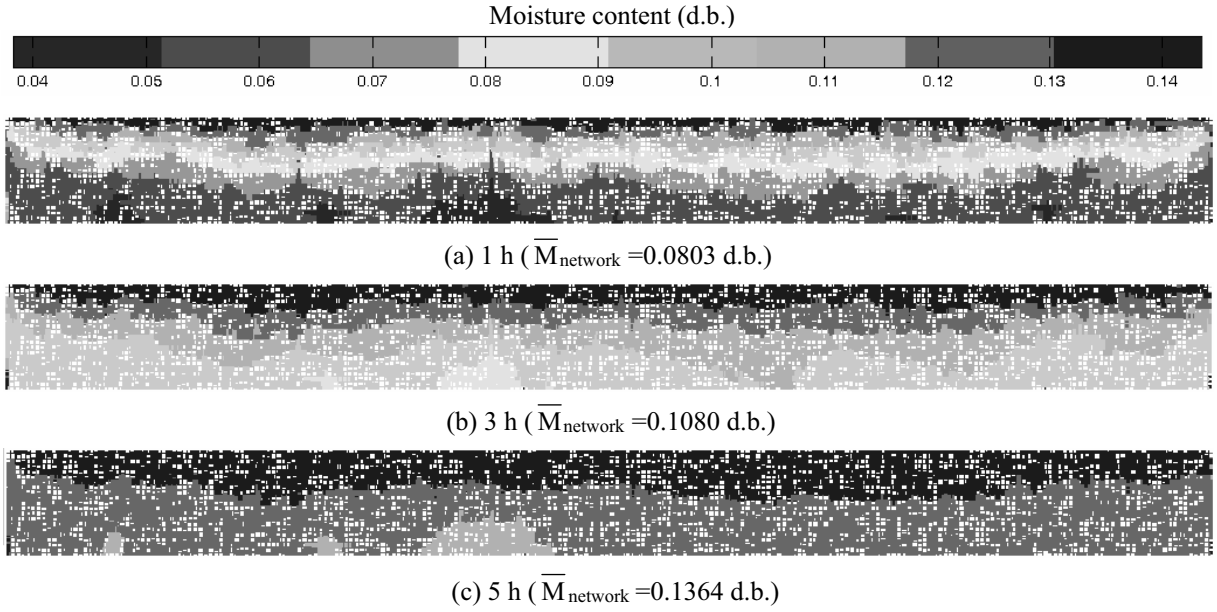

(a) 1 h ($\overline{M}_{network}$ =0.0803 d.b.)

(b) 3 h ($\overline{M}_{network}$ =0.1080 d.b.)

(c) 5 h ($\overline{M}_{network}$ =0.1364 d.b.)

Fig. 10. Visualization of moisture contents in pores of banana foam at temperature of 35^{o}C, initial foam density of 0.3 g/cm^3 and relative humidity of 50%

This value was in a normal range of porous materials (adsorbents and catalysts) for which the tortuosity factor varies between 2 and 6, corresponding to the porosity between 0.3 and 0.8 (Aguilera and Stanley, 1999)

Validation

As previously shown in Figures 2 and 3, the pore network model showed a good fit to the experimental data throughout the exposure time, with R^2-values above 0.98 at the relative humidity below 67%. Beyond 67%, however, the lower accuracy of prediction was found (R^2 values varying between 0.96-0.97); the model predicted the change of moisture content of sample relatively faster than the experiment at the early exposure time and became relatively slower at the later time.

Graphic visualization

Figure 10 shows the moisture distribution in 2-D pore network during adsorption process. Each pore was colored according its moisture content. The representative colours with 8 shades from red to blue were used for corresponding range of moisture from 0.038 to 0.138 d.b.

At the beginning, every pore within the network presumably contained the moisture content of 0.038 d.b. After 1 hour of adsorption, it can be seen in Figure 10a that the adsorption front moved from the top to the bottom and this confirmed the assumption used in the model. Moisture content near the surface reached the equilibrium value of 0.138 d.b. whilst the moisture content near the bottom was approximately 0.05-0.06 d.b., indicating that the liquid water only forms a thin liquid film near the pore walls and moisture transfer processes at this time may be dominated by molecular vapour diffusion.

In addition, it is clear from Figure 10 that the pattern of increasing moisture content at the same horizontal plane for a given time was irregular, reflecting the pore structure effect. As a result, the moisture contents were quite different and this can be seen clearly at the bottom surface of the pore network for the exposure time of 3 hours as an example, showing the moisture content of approximately 0.08-0.09 d.b in a small area as indicated by yellow colour (see Figure. 10b) whilst the other areas at the bottom surface were coloured by green corresponding to the moisture contents of 0.095-0.105 d.b. For the region of lower moisture content, the pores positioned at that region were relatively larger in sizes than the surrounding nearby pores. Hence, the moisture diffusing through those large pores was restricted by the smaller ones since the cross sectional area available for moisture diffusion is reduced in the surrounding nearby small pores.

CONCLUSIONS

- A 2-D stochastic pore network has been developed to represent the pore structure of banana foam and the transport of water vapour in the pores of the network was described by Fick's second law. The optimization technique with a

golden-search method was used to determine the diffusivity of pores. The experimental results showed that the pore network model could describe the moisture migration inside banana foam relatively well.

- The interactions between pore structure and moisture movement were relatively complicated and the visualization using colour coded moisture content helped understanding of their interactions.
- The pore diffusivity at a given temperature insignificantly changed with the relative humidities, except for the higher relative humidities of 70% at which the diffusivity had a decreasing trend. Moreover, the pore diffusivity depended strongly on the temperature, but was independent of the initial banana foam densities.

NOMENCLATURE

a_w	water activities	-
D_{eff}	effective diffusivity	m^2/s
D_A	actual diffusivity in the pore voids	m^2/s
D_p	apparent pore diffusivity	m^2/s
h_m	convective mass transfer coefficient	m/s
L	pore length	m
M	moisture content (dry basis)	kg/kg^{-1}
N	number of interval	-
$r_{i,j}$	pore radius	m
RH	relative humidity	%
RMSE	root mean square error	-
t	adsorption time	s
T	temperature	^oC
x	distance along the pore length	m
Z	number of pores in the network	-

Greek letters

ε	porosity	-
τ	tortuosity factor	-
ρ	initial foam density	g/cm^3

Subscripts

i	initial
m	mass
e	equilibrium
exp	experimental
s	surface

ACKNOWLEDGEMENTS

The authors express their appreciation to the Commission on Higher Education and the Thailand Research Fund (TRF) for financial support.

REFERENCES

Aguilera, J. M., Stanley, D. W. (1999), Microstructural principles of food processing and engineering. Aspen Publishers Inc, Maryland.

Androutsopoulos, G.P. and Mann, R. (1979), Evaluation of mercury porosimeter experiments using a network pore structure model, Chemical Engineering Science, Vol. 34, pp. 1203-1212.

Blunt, M. (2001), Flow in porous media-pore-network models and multiphase flow, Current Openion in Colliod & Interface Science, Vol. 6, pp. 197-207

http://www.intel.com/cd/software/products/asmo-na/eng/compilers/284132.htm

Hollewand and Gladden, L.F. (1992), Modeling of diffusion and reaction in porous catalysts using a random three-dimensional network model, Chemical Engineering Science, Vol. 47, pp. 1761-1770.

Jamali, A., Kouhila, M., Mohamed, L. A., Idlimam, A., Lamharrar, A. (2006), Moisture adsorption–desorption isotherms of citrus reticulata leaves at three temperatures, Journal of Food Engineering , Vol. 77, pp. 71–78.

Kaya, S., Kahyaoglu, T. (2005), Thermodynamic properties and sorption equilibrium of pestil (grape leather), Journal of Food Engineering, Vol.71, pp. 200-207.

Kim, M. K., Okos, M., R. (1999), Some physical, mechanical, and transport properties of crackers related to checking phenomenon, Journal of Food Engineering, Vol. 40, pp. 189-198.

Labuza, T.P., Hyman, C.R. (1998), Moisture migration and control in multi-domian foods, Food Science and Technology, Vol. 9, pp. 47-55.

Mann, R. (1993), Developments in chemical reaction engineering: issues relation to particle pore structures and porous materials, Chemical Engineering Research and Design, Vol. 71, pp. 551-562.

Palou, E., Lopez-Malo, A., Argiz, A. (1997) Effect of temperature on the moisture sorption isotherms of some cookies and corn snacks, Journal of Food Engineering , Vol. 31, pp. 85-93.

Prachayawarakorn, S., Prakotmak, P., Sopornronnarit, S. (2008), Effect of pore size distribution and pore-architecture assembly on drying characteristics of pore networks, International Journal of Heat and Mass Transfer, Vol. 51, pp. 344-352.

Roca, E., Guillard, V., Guilbert, S., Gontard, N. (2006), Moisture migration in a cereal composite food at high water activity: Effects of initial porosity and fat content, Journal of Cereal Science, Vol. 43, 144-151.

Segura, L.A., Toledo, P.G. (2005), Pore-level modeling of isothermal drying of pore networks:

Effects of gravity and pore shape and size distributions on saturation and transport parameters, Chemical Engineering Journal, Vol. 111, pp. 237-252.

Yiotis, A.G., Stubos, A.K., Boudouvis, A.G.,Tsimapanogiannis, I.N, Yortsos, Y.C. (2005), Pore-network modeling of isothermal drying in porous media. Transport in Porous Media, Vol. 58, pp. 63-86.

EFFECT OF MOISTURE ADSORPTION ON EFFECTIVE DIFFUSIVITY AND TEXTURAL PROPERTY OF BANANA FOAM MAT

*Preeda PRAKOTMAK[1], Somkiat PRACHAYAWARAKORN[2] and Somchart SOPONRONNARIT[1]

[1] *School of Energy, Environment and Materials, King Mongkut's University of Technology Thonburi*
126 Pracha u-tid Road, Bangkok 10140, Thailand

[2] *Department of Chemical Engineering, King Mongkut's University of Technology Thonburi*
126 Pracha u-tid Road, Bangkok 10140, Thailand

Corresponding author: Somkiat PRACHAYAWARAKORN. E-mail: somkiat.pra@kmutt.ac.th

Keywords: adsorption kinetics; banana foam mat; crispness; effective moisture diffusivity

ABSTRACT

Foam-mat drying technique can improve the mass transfer rate. However, the high porous of dried product could quickly adsorb the moisture from the air during storage, leading to the lost of textural property. The main purpose of this research was therefore to study moisture adsorption kinetics of banana foam mat and its quality. The adsorption isotherms experiments were carried out with standard static method using saturated salt solutions over a wide range of relative humidities from 31 to 82%, and a temperature range of 35 to 45°C. Two different banana foam densities of 0.21 and 0.26 g/cm^3 were used to adsorb water vapor under the controlled conditions. A Fick's second law and the optimization technique were used to estimate the effective moisture diffusivity (D_{eff}) at adsorption conditions. Three empirical equations i.e. a power-law, and two exponential forms for describing the dependence of the effective moisture diffusivity on moisture content were tested. The power-law function was suitably described the variation of the effective moisture diffusivity with moisture content. The force deformation curve obtained from a penetration test of the samples showed that an increase of moisture content of sample decreased number of peaks and initial slope.

INTRODUCTION

The foam mat drying can enhance the drying rate of banana since its structure is very porous. The textural properties in particular hardness and crispiness are better in the dried foamed banana than the non foamed banana; the foamed banana provides less hardness and more crispy. However, the product is very hygroscopic and its texture could be lost quickly if it keeps undergoing undesirable condition. To circumvent the undesirable property, the understanding of moisture adsorption for the banana foam at conditions is necessary. Application of food texture analysis and moisture diffusivity will help to improve food product quality adsorption conditions and understand the movement of moisture.

Many dry crispy products are sensitive to moisture migration. Moisture transport in porous foods is very complicated since the pore system is very complex and irregular. Generally, the diffusion of gases or liquids through the complex structure can be simply described by classical Fick's second law in which the overall mass transports are lumped into an effective diffusivity. The wide ranges of effective moisture diffusivity in different physical structure of food materials have been reported in the literature [1] and it has been known to be either independent or function of moisture content. Nevertheless, general model for evaluating the effective diffusivity of food materials have not existed [2]. Many empirical such as power-law, polynomial and exponential forms were frequently used to describe the relation of effective moisture diffusivity with moisture content in the foodstuffs [3, 4 and 5]. The different result in effective moisture diffusivity values would be attributed to the difference in food structure.

The objectives of this study were to select a suitable empirical equation of effective moisture diffusivity, to investigate the influence of relative humidity, temperature and initial foam density on the effective moisture diffusivity. The effect of moisture content on product textures was also determined. The textural property was characterized by initial slope, number of peaks and maximum force.

DRIED BANANA FOAM PREPARATION

The banana puree with 5% of fresh egg albumen used as foaming agent were foamed to density of 0.3 and 0.5 g/cm^3. The density was determined by measuring the mass of a fixed volume of the foam. The banana foams was poured slowly into a steel block and then placed on a mesh tray, which was covered with aluminium foil. After that, it was dried to about 3% kg/kg d.b. using 80°C and a 0.5 m/s superficial air velocity. The banana foam prepared from the initial foam densities of 0.3 and 0.5 g/cm^3 can produce the dried banana densities of 0.21 ± 0.02 and 0.26 ± 0.02 g/cm^3, respectively. The product thicknesses after drying were 2.8 mm and 3.2 mm for the densities of 0.21 and 0.26 g/cm^3, respectively. Five replicates were performed.

ADSORPTION EXPERIMENT

Moisture adsorption experiments were carried out using the static method. Samples were placed into the glass jars contained the saturated salt solutions ($MgCl_2$ $6{\cdot}H_2O$, $Mg(NO_3)_2$ $6{\cdot}H_2O$, KI, NaCl and KCl) which provided the relative humidity (RH) in range of 32-82% at the temperatures of 35, 40 and 45°C. All the jars were placed in the temperature-controlled oven at the operating temperature with a precision of ±1°C (UFE500, Memmert, Germany). Samples were weighed at different exposure

times ranging from 1 to 120 h. At RH > 74%, a small amount of toluene held in a vial was fixed in the glass jars in order to prevent microbial spoilage of the samples [6]. Moisture content of each sample after reaching the equilibrium condition was determined by drying it with the hot air oven at a temperature of 103°C for 3 h. The moisture content determined by the hot air oven was used instead of the AOAC method [7], the percentage error from two methods approximately 0.4% [8]. The experiment at each sorption condition was repeated three times and the mean value was reported.

SEM PHOTOGRAPH

The morphologies of dried banana foam mats were characterized using scanning electron microscope (SEM) with an accelerating voltage of 10 kV. Before photographing, the specimens were cut into a dimension of 5 × 5 mm and then glued on the metal stub. The samples were coated with gold, scanned, and photographed at 15X magnification

TEXTURE ANALYSIS

The effects of moisture content on product textures were studied. The initial moisture content of the banana foam was about 0.038 kg/kg d.b. The dried banana foam mats adsorbed water vapour in the glass jars which controlled relative humidity about 75% by using saturated NaCl solutions at temperature of 24°C. After moisture adsorbed for determined time, the test applied a direct force to the sample using a 5 mm spherical probe at a constant crosshead speed of 2 mm/s. The hardness was defined as the maximum force of the force-deformation curve and the crispness was characterized by the number of peaks and the slope of the first peak. The data were analyzed by ANOVA using Duncan's multiple range test at $p<0.05$. Eight samples were tested and the average values of hardness and crispness were presented. Moisture content of each sample after the texture analysis was determined. All experiments were performed at 24°C.

DETERMINATION OF EFFECTIVE MOISTURE DIFFUSIVITY

The banana foam mats used in the experiments has a dimension of 43 × 43 × 4 mm. This sample size may provide the transport of moisture in direction of thickness. The transport of moisture can be described by Fick's equation:

$$\frac{\partial M(x,t)}{\partial t} = \frac{\partial}{\partial x}\left(D_{eff}(M)\frac{\partial M(x,t)}{\partial x} \right) \quad (1)$$

or

$$\frac{\partial M(x,t)}{\partial t} = D_{eff}(M)\frac{\partial^2 M(x,t)}{\partial x^2} + \frac{\partial M(x,t)}{\partial x}\cdot\frac{\partial D_{eff}(M)}{\partial x} \quad (2)$$

where $D_{eff}(M)$ is the effective moisture diffusion coefficient (m^2/s), M the moisture content (kg/kg d.b.), t the time (s) and x the distance along the diffusion path (m). In this study, it was assumed that the initial moisture distribution inside the sample was spatially uniform and the migration of water vapor from the surrounding air to the foam mat surface occurred at the top surface and no moisture transferred at the bottom since the sample surface was placed on an opaque glass dish. Initial moisture distribution in the sample was assumed to be uniform. From the above assumptions, the following initial and boundary conditions can be setup:

$$M(x,t) = M_{in} \quad 0 \le x \le L \ at\ t = 0 \quad (3)$$

$$D_{eff}(M)\left(\frac{\partial M(L,t)}{\partial x}\right) = h_m\left(M_e - M_s\right) \quad x = 0 \ at\ t > 0 \quad (4)$$

$$\frac{\partial M(x,t)}{\partial x} = 0 \quad x = L \ at\ t > 0 \quad (5)$$

where M_{in} is the initial moisture content (kg/kg d.b.), M_s and M_e the moisture content at the surface and at the equilibrium (kg/kg d.b.), respectively, L thickness of material (m), h_m the convective mass transfer coefficient (m/s). Eqs. (2), (4) and (5) can be, respectively written in a finite difference form as follows:

$$\frac{M_i^{t+1} - M_i^t}{\Delta t} = D_i\left(\frac{M_{i+1}^t - 2M_i^t + M_{i-1}^t}{(\Delta x)^2}\right) + \left(\frac{M_{i+1}^t - M_{i+1}^t}{2\Delta x}\right)\left(\frac{D_{i+1}^t - D_{i-1}^t}{2\Delta x}\right) \quad (6)$$

$$D_N^t\,\frac{M_N^{t+1} - M_{N-1}^{t+1}}{\Delta x} = h_m\left(M_e^{t+1} - M_N^{t+1}\right) \quad (7)$$

$$\frac{M_0^{t+1} - M_0^t}{\Delta t} = 2D_0^t\left(\frac{M_{i-1}^t - M_i^t}{(\Delta x)^2}\right) \quad (8)$$

In the calculation of moisture content, the sample thicknesses of 2.8 and 3.2 mm for the respective foam densities of 0.21 and 0.26 g/cm^3 were divided in 105 and 120 layers and the time step of 0.01 sec was chosen.

After the moisture content at every node is known, the average moisture content $\overline{M}(t)_{pre}$ can be readily be calculated by integrating the predicted moisture profile though out the sample thickness and the trapezoidal numerical integration was used:

$$\overline{M}(t)_{pre} = \frac{\left(M_0^t + M_N^t + 2\sum_{i=1}^{N-1} M_i^t\right)\Delta x}{2L} \quad (9)$$

where N is number of layer. The dependence of diffusivity on moisture content can not be described by any specific equation. To find the suitable form of equation, three possible empirical equations obtained from the literature [9, 10, and 11] were tested with the moisture adsorption data.

$$D_{eff}(M) = D_0 \exp\left(-\left(e_1 M + e_2 M^2\right)\right) \quad (10)$$

$$D_{eff}(M) = D_0 \cdot M^{D_x} \quad (11)$$

$$D_{eff}(M) = D_0 \exp(-a \cdot M) \quad (12)$$

where D_0, D_x, e_1, e_2, and a are the constant parameters.

The accuracy of the models was evaluated by root mean square error (RMSE) and coefficient of determination (R^2) value. The RMSE is defined as

$$RMSE = \left[\frac{1}{P} \sum_{n=1}^{P} (M(t)_{\exp} - \overline{M}(t)_{pre})^2 \right]^{1/2} \quad (13)$$

where $M(t)_{\exp}$ is the experimental average moisture content of material at time t, $\overline{M}(t)_{pre}$ the predicted average moisture content and P the number of experimental data. The lower the value of RMSE is the better the goodness of fit. In this work, a modified Nelder-Mead simplex method was used to estimate the constant parameters in Eqs. (10), (11) and (12). The RMSE was set as the objective function with a tolerance of 10^{-9}. The initial guesses obtained by least squares fits of the data calculated from the method of slopes [12]. The model with the lowest value of RMSE and highest value of R^2 was considered the best model to correlate the experimental data. The code for numerical solution was written in Microsoft Visual C++ 6.0 programming language. All computations were implemented using Intel C++ Compiler [13] and run on a PC with 3.0 GHz.

RESULTS AND DISCUSSION

Identification of effective moisture diffusivity model

To find the appropriate diffusion equation, two sets of the moisture adsorption data at 40°C and 66% RH as well as at 35°C and 83% RH were demonstrated. The estimated constant parameters for Eqs (10), (11) and (12) along with their values of RMSE and R^2 are presented in Table. 1. The R^2-value for all diffusion models is above 0.99 and the values of RMSE were lower than 0.007. When using these constant parameters for calculating the moisture content, it was found that all diffusion models can predict moisture content in agreement with the experiment as can be seen in Figs. 1a and 1d.

Table 1 Estimated parameters of empirical models for selected conditions

Estimated parameters	Experimental conditions					
	40 °C, 66% RH			35 °C, 83% RH		
	Eq.(10)	Eq.(11)	Eq.(12)	Eq.(10)	Eq.(11)	Eq.(12)
D_0	5.947×10^{-10}	8.908×10^{-11}	3.962×10^{-10}	1.709×10^{-10}	6.326×10^{-11}	1.236×10^{-10}
e_1	11.108	-	-	4.604	-	-
e_2	-27.508	-	-	-7.172	-	-
D_x	-	-0.463	-	-	-0.244	-
a	-	-	-3.914	-	-	-1.210
R^2	0.996	0.999	0.998	0.995	0.999	0.998
RMSE	0.0035	0.00101	0.00114	0.0065	0.00306	0.00336

However, when considering moisture diffusivity obtained from the models, it can be seen from Figs 1c and 1f that the diffusivity values of all diffusion models decrease with increasing moisture content. According to theses results, it implied that difference in the values of effective moisture diffusivity determined from the models was insensitive to the calculation of moisture content; the moisture contents calculated using the diffusion models were almost superimposed. Hence, it is very difficult to identify the suitable model for predicting the moisture content based on the values of RMSE and R^2, and one more criterion was used to quantify the quality of estimated constant parameters.

The local relative error (E) was used to identify the suitable diffusion model and it is defined as

$$E(t) = 100 \frac{\left| M_{\exp}(t) - M_{calc}(t) \right|}{M_{\exp}(t)} \quad (14)$$

where $M_{exp}(t)$ is the experimental moisture content at time t and $M_{calc}(t)$ is the moisture content from prediction. If the estimation of moisture content is perfect, the value of E at time t is zero. The values of E for the three empirical diffusion models are shown in Figs. 1b and 1e, indicating that the value of E was less than 1% throughout the exposure time when the relationship between effective moisture diffusivity and moisture content was described by Eq. (11) whilst the error from prediction by using other equations were higher than 1 %.

The prediction of adsorbed moisture content at the early period with high accuracy is very important to crispy product since the product quickly loses its crispy texture when the product adsorbs the water vapor up to certain moisture content. From this study, the banana foam will lose crispiness at moisture content about 5% d.b. as can be seen in section of texture banana foam. From these results, it can be deduced that Eq. (11) is reasonably used to describe the moisture adsorption of banana foam. This power-law model is also used to describe moisture adsorption in the snack foods such as sponge cake [14], showing the similar tend of moisture diffusivity with moisture content.

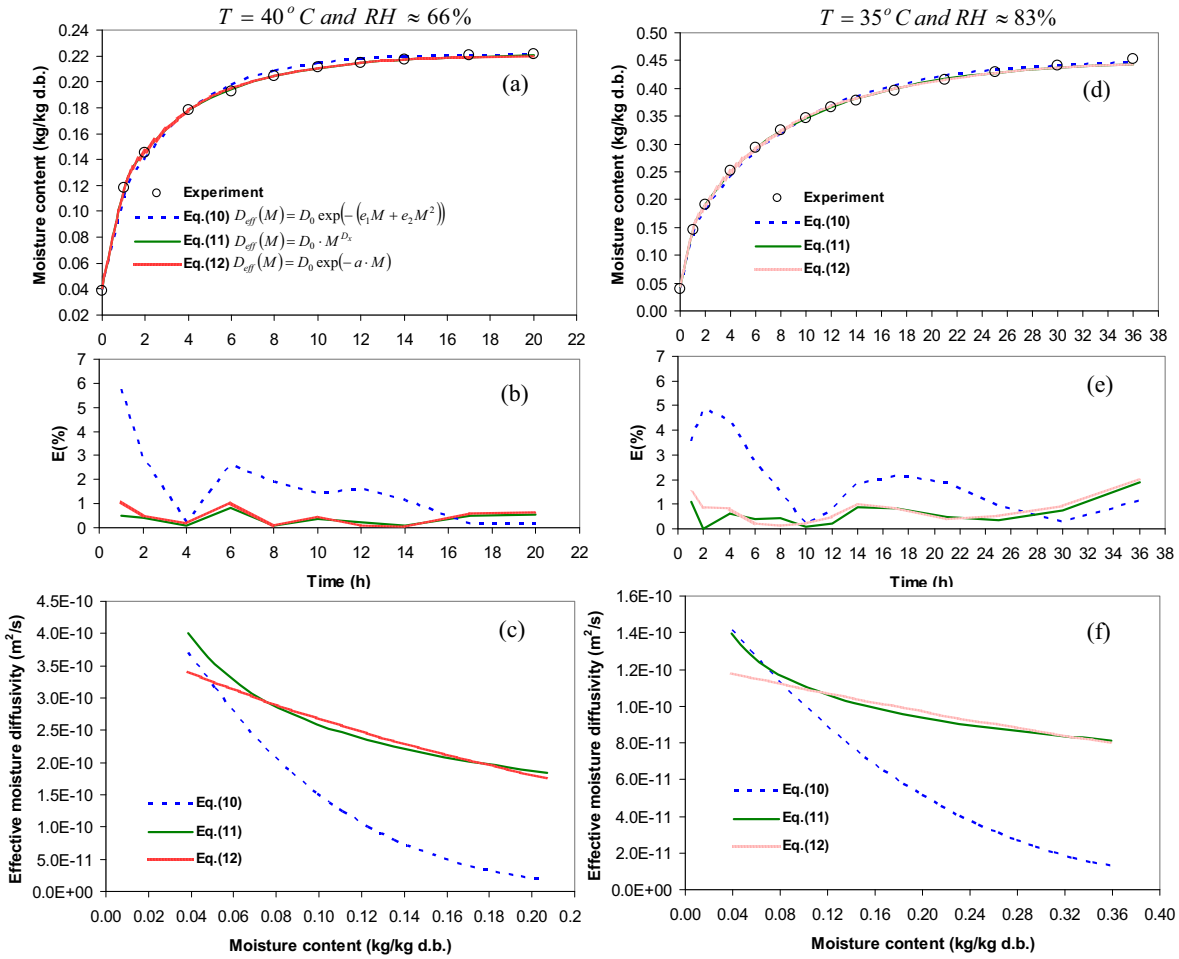

Fig. 1. Validation of the moisture uptake estimated and the variation of effective diffusion coefficient with moisture content of two selected cases

Effect of relative humidity on effective moisture diffusivity

Fig. 2 shows the moisture adsorption at 35°C and relative humidity of 32 to 83% for the banana foam density of 0.21 g/cm^3. As expected, the faster adsorption rate was accomplished with higher relative humidity. The predictions of moisture content using Eqs. (1) and (11) agreed well with experimental data over a wide range of relative humidities.

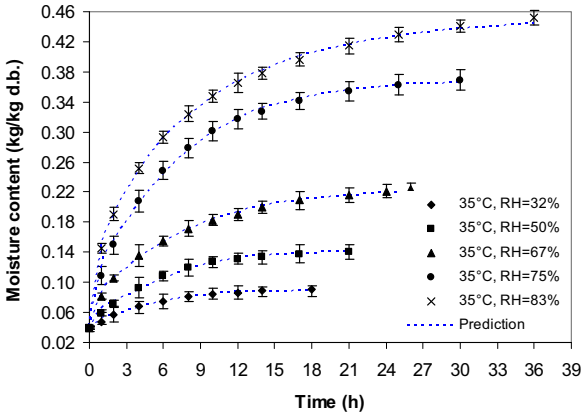

Fig. 2. Effect of relative humidities on moisture adsorption kinetics at 35°C for the foam density of 0.21 g/ cm^3

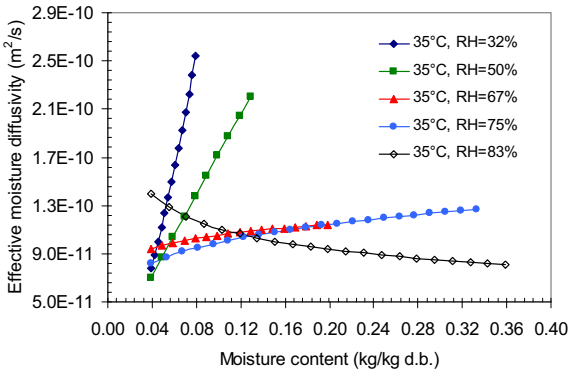

Fig. 3. Variation of effective diffusion coefficient with moisture content at various relative humidities for the dried banana foam density of 0.21 g/cm^3

Fig. 3 shows the changes of D_{eff} with moisture content at 35°C and at different relative humidities. The trend of changing D_{eff} with moisture content was very different amongst relative humidities. The values of D_{eff} remarkably increased with increasing moisture content at relative humidity of 32% and when the relative humidity increased continually, the change of D_{eff} with moisture content became smaller, as indicated by a lower slope,

until at relative humidity of 83% the D_{eff} trend was reversed, showing a decrease in D_{eff} when the sample adsorbed water vapor. The D_{eff} trends at other temperatures such as 40 and 45°C were similar to Fig.3, but the tendency for D_{eff} to decrease with moisture content occurred at lower relative humidity (66% RH at 40-45°C).

Such different trends of D_{eff} can be explained by the fact that at the relative humidity of 32% the water vapour can diffuse rapidly through the voids of the banana foam mats and is then adsorbed onto the pore wall. Since the equilibrium moisture content at this relative humidity is very low (< 0.13 kg/kg d.b.), the moisture content at this level is called bound water. The molecular mobility of bound water increases with the level of moisture content. Hence, the increase of D_{eff} with increasing moisture content could be attributed to contributions from diffusion in the solid matrix of food and vapour diffusion in pores.

When the relative humidity increased, the water vapor molecules frequently collide amongst themselves in the pore space and the condensation of water vapor may occur inside the pore spaces in particular small pores. The occurrence of condensation is due to the increasing van der Waals interactions between vapor molecules inside pore space. When the pores inside the porous food are filled with the condensed water, the water vapour cannot diffuse through these pores and this, in turn, provides the smaller flux of water vapor diffusing through the porous food. Hence, the D_{eff} decreased. As shown in Fig. 3, for example, when compared at the same moisture content, the value of D_{eff} was significantly lower at relative humidity of 50% than at 75%. From the condensation effect, the change of moisture diffusivity with moisture content became smaller at higher relative humidity.

At the relative humidity of 83% at which the banana foam surface of banana foam started getting wet at moisture content of approximately 0.12 kg/kg d.b. This may cause a sharp decrease of D_{eff} for the moisture range of 0.04 kg/kg d.b. to 0.12-0.16 kg/kg d.b. Beyond this range, the D_{eff} changed slightly, implying that the transport of moisture is contributed from the liquid diffusion.

Effect of temperature and initial foam density on effective moisture diffusivity

Fig. 4 shows the changes of D_{eff} at 35 and 40°C. As expected, the D_{eff} increased with increase in temperature.

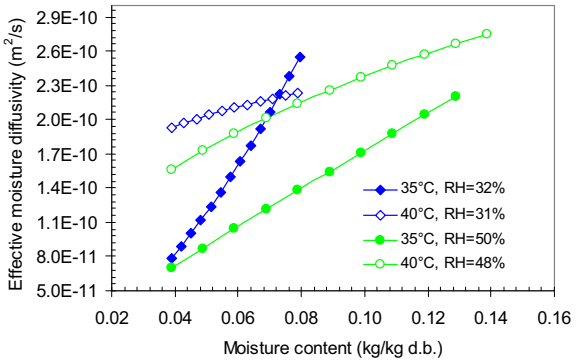

Fig. 4. Effect of temperatures on the D_{eff} at the foam density of 0.21 g/cm^3

Fig. 5 shows the D_{eff} value for both foam densities at an illustrated temperature of 35°C for the relative humidities approximately 32 and 50%. As shown in this figure, at the same relative humidity, the D_{eff} was slightly lower at the foam density of 0.26 g/cm^3 than at the density of 0.21 g/cm^3. The difference in the D_{eff} can be accounted for the morphology difference among both samples as can be seen in the SEM.

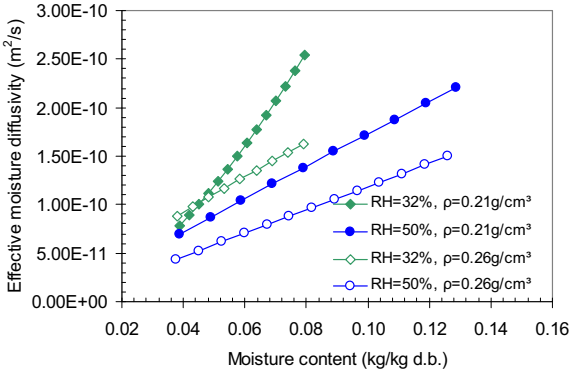

Fig. 5. Effect of initial foam densities on D_{eff} at the temperature of 35°C

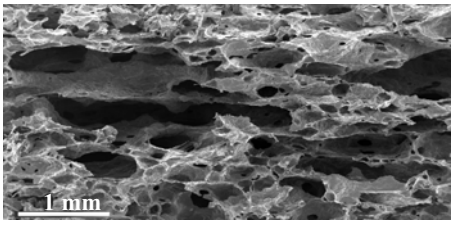

(a) 0.21 g/cm^3

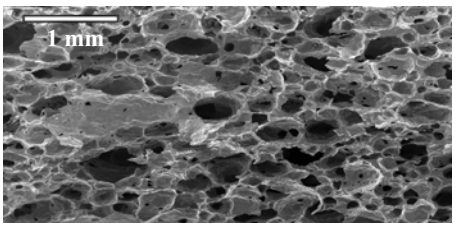

(b) 0.26 g/cm^3

Fig. 6. SEM micrographs of dried banana foam mats at different initial foam densities

The microstructures of dried banana foam mats characterized by SEM are shown in Figs. 6a and 6b for two initial foam densities. It is clear from these figures that the sample with an initial foam density of 0.21 g/cm^3 had larger pore than higher foam density. In the porous banana foam studied, the void area fractions for the banana foam densities of 0.21 and 0.26 g/cm^3 were 31 and 26 %, respectively. High porosity in porous foods provides less diffusional flux resistance and thus greatly facilitates the moisture transport to those porous foods.

Texture of banana foams

Fig. 7 shows the curves of the force measured versus displacement recorded by texture analyzer at different moisture content levels. As observed from this figure, the maximum force decreased with increasing the moisture content levels. The jagged pattern of the force-deformation

curve reflects the higher crispy behavior of the banana foam mats. When the sample was adsorbed more moisture, this fracture pattern was absent, revealing the sample is not expected to have the crisp and hard eating character.

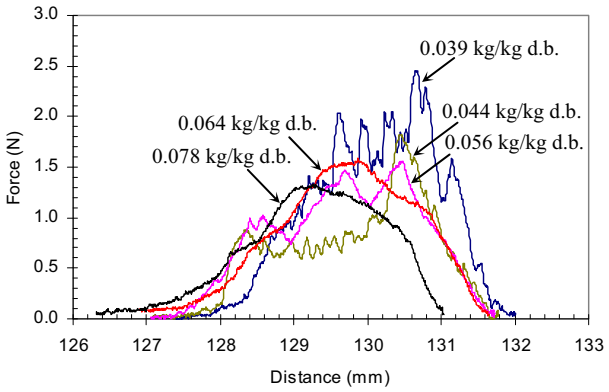

Fig. 7. Variation in force-deformation curve during compression test at various moisture content levels for foam density of 0.21 g/cm^3

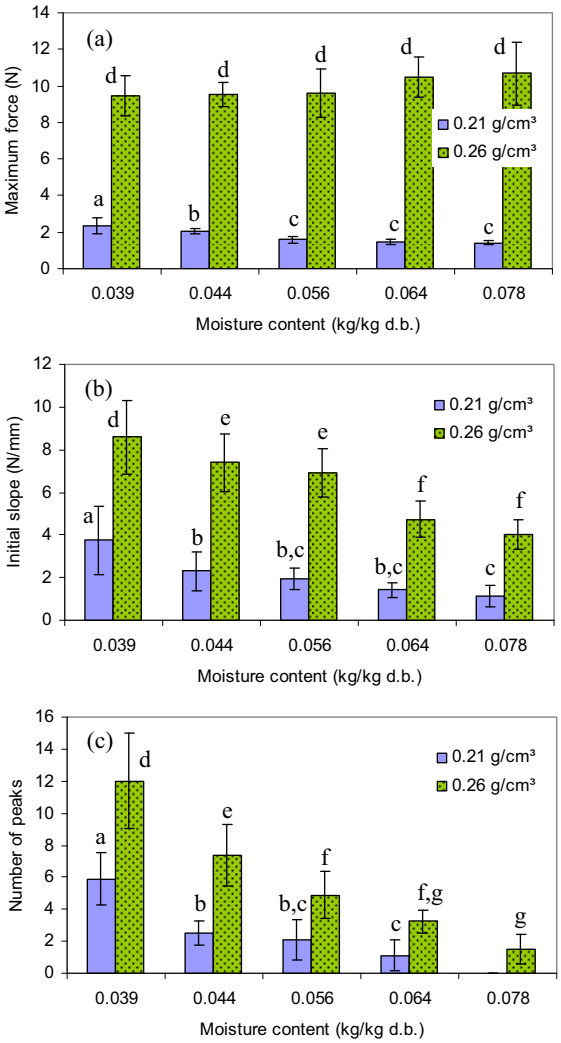

Fig. 8. Effect of moisture content and initial foam densities on (a) maximum force, (b) initial slope and (c) number of peaks of the banana foam mats

The textural parameters such as maximum force, initial slope and number of peaks are determined from force-deformation curve and the results are shown in Fig. 8. The number of peaks was counted when the force amplitude is more than the threshold values, which was set at 30 g. The statistical analysis results were also shown in Figs. 8b and 8c. The number of peaks and initial slope for both foam densities significantly decreased with increasing moisture content, but the maximum forces of each initial foam densities were insignificantly different when the moisture content increased. The number of peaks for both foam densities approaches zero at moisture content of about 0.078 kg/kg d.b., which indicate that the product lost all its characteristic crispness.

In the tropical countries such as Thailand, the relative humidity was around 65-73%. At this range of relative humidity, the equilibrium moisture content of the banana foam was approximately 0.24-0.36 kg/kg d.b. Hence, the banana foam mat can lose its textures. To maintain the crispy texture of product, the banana foam should be kept at low relative humidity or kept with a good packing system.

CONCLUSION

An optimization technique using Nelder-simplex method was applied to estimate the effective moisture diffusivity. Three empirical equations describing the dependence of the effective moisture diffusivity on moisture content were tested. The statistical analysis shows that a power law function suitably described the relationship of the effective moisture diffusivity with moisture content in banana foam mat. The relative humidity strongly affected the moisture diffusion mechanisms as indicated by the subtle changes of effective moisture diffusivity at conditions. In addition to the moisture content and relative humidity, the effective moisture diffusivity depended on the temperature and foam density. As the banana foam adsorbed water vapor, the number of peaks and initial slope decreased, but the maximum force did not change.

ACKNOWLEDGMENTS

The authors would like to express their appreciation to the Commission on Higher Education, Thailand for supporting by grant fund under the program Strategic Scholarships for Frontier Research Network for the Ph.D. Program Thai Doctoral degree for this research. This work was also supported in part by the Thailand Research Fund and King Mongkut's University of Technology Thonburi.

REFERENCES

1. Tong, C.H. and Lund, D.B. Effective moisture diffusivity in porous materials as a function of temperature and moisture content. Biotechnol. Prog. 6: 67-75 (1990)
2. Saravacos, G.D. and Maroulis, Z.B. Transport properties of foods, Marcel Dekker, New York (2001)

3. Zogzas, N.P., Maroulis, Z.B. and Marinos-Kouris, D. Moisture Diffusivity Data Compilation in Foodstuffs. Drying Technology. 14: 2225-2253 (1996)
4. Loulou, T., Adhikari, B. and Lecomte, D. Estimate of concentration-dependent diffusion coefficient in drying process from the space-average concentration versus time with experimental data. Chemical Engineering Science. 61: 7185-7198 (2006)
5. Bourlieu, C., Guillard, V., Powell, H., Vallès-Pàmies, B., Guilbert, S., and Gontard, N. Modelling and control of moisture transfers in high, intermediate and low a_w composite food. Food Chemistry. 106: 1350-1358 (2008)
6. Kaya, S. and Kahyaoglu, T. Thermodynamic properties and sorption equilibrium of pestil (grape leather). Journal of Food Engineering. 71: 200-207 (2005)
7. AOAC. Official Methods of Analysis, 16th ed, Association of Official Agricultural Chemists, Washington, DC (1995)
8. Thuwapanichayanan, R., Prachayawarakorn, S., and Sopornronnarit, S. Modeling of diffusion with shrinkage and quality investigation of banana foam mat drying. Drying Technology. 26: 1326-1333 (2008)
9. Olek, W. and Weres, J. Effects of the method of identification of the diffusion coefficient on accuracy of modeling bound water transfer in wood. Transport Porous Media (2006)
10. Guillard, V., Broyart, B., Bonazzi, C., Guilbert, S. and Gontard, N. Moisture diffusivity in sponge-cake as related to porous structure evaluation and moisture content. Journal of Food Science. 68: 555-562 (2003)
11. Sakin, M., Kaymak-Ertekin, F., and Ilicali, C. Modeling the moisture transfer during baking of white cake. Journal of Food Engineering. 80: 822-831 (2007)
12. Karathanos, V. T., Villalobos, G., and Saravacos, G. D. Comparison of two methods of estimation of the effective moisture diffusivity from drying data. Journal of Food Science. 55: 218-233 (1990).
13. Intel® Software Network. Available (2009) at: http://www.intel.com/cd/software/products/asmo-na/eng/368972.htm
14. Roca, E., Guillard, V., Guilbert, S. and Gontard, N. Moisture migration in a cereal composite food at high water activity: Effects of initial porosity and fat content, Journal of Cereal Science. 43: 144-151 (2006)

10 Superheated-Steam Drying Applied in Food Engineering

Somkiat Prachayawarakorn
and Somchart Soponronnarit

CONTENTS

10.1 INTRODUCTION

The primary aim of food drying is to preserve the product, as a decrease in the product moisture content can prevent the growth of microorganisms and enzymatic reactions. However, drying may have an adverse effect on physical, chemical, and nutritional values of food products. The success or failure of a drying process depends on the product quality obtained after drying and also on the efficiency of the process.

An idea of using superheated steam instead of hot gas (air, combustion, or flue gases) for drying was initially introduced in Germany in 1908 as reported by Douglas (1994), but its application was limited to only a few industries. Later, its use has widely been acknowledged in many applications, i.e., paper (Svensson, 1980; Douglas, 1994), foods (Iyota et al., 2001; Taechapairoj et al., 2003; Tang et al., 2005),

coal (Chen et al., 2000), and wood (Pang and Dakin, 1999). The product quality after drying is usually better in superheated-steam drying (SSD) than in hot-air drying, particularly in terms of less shrinkage and higher product porosity.

A superheated-steam dryer is normally designed as a closed loop in which exhaust steam may be either reused or employed in other processes resulting in net energy savings. The temperature of superheated steam used under atmospheric pressure generally varies between 100°C and 150°C. The high temperature restricts its application to foods that are not sensitive to heat. Mostly, the applications of SSD are related to starch-based products such as parboiled rice, noodles, potato chips, and durian chips (Iyota et al., 2001; Markowski et al., 2003; Taechapairoj et al., 2004; Jamradloedluk et al., 2007).

In this chapter, the basic concepts of SSD, drying characteristics, mathematical modeling of the process operation, and quality consideration of the selected food products are outlined and discussed.

10.2 ADVANTAGES AND LIMITATIONS OF SUPERHEATED STEAM DRYING

When water in a liquid state is contained in a closed vessel and heated under a given pressure, its temperature increases up to the boiling point as shown in Figure 10.1. At this point, water is called saturated liquid (shown by letter a in Figure 10.1). Upon continued heating, the temperature would remain constant at that saturation value and water would continually vaporize. During this heating period, the system contains two phases, liquid and vapor. After the last droplet of water vaporizes, there is only water vapor in the system, which is called saturated steam (shown by letter b in Figure 10.1). From a practical viewpoint, saturated steam cannot be used to dry any materials since the steam is wet. To obtain dry or superheated steam, saturated steam

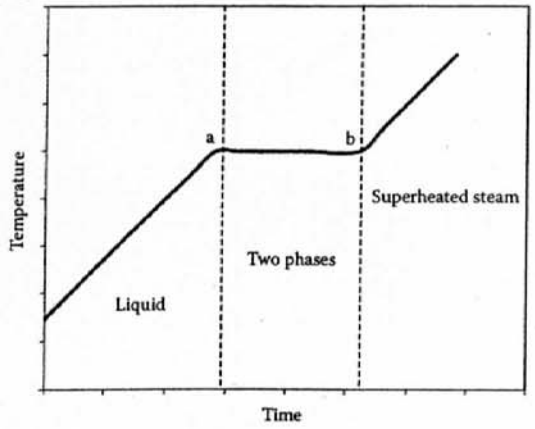

FIGURE 10.1 Illustration of changing states of water during heating.

needs to be further heated by flowing it through a heat exchanger. As a result, the temperature of steam increases beyond its saturation temperature. The temperature difference between superheated and saturated steam is called degree of superheat.

Using superheated steam in an industrial process can lead to substantial energy savings if the vapor evaporating from the product being dried is condensed and if the latent heat of condensation can be recovered and used in other unit operations. This benefit makes superheated steam a more attractive drying medium for industrial use, especially if the energy cost for drying is a major proportion of the total production cost. In addition, the use of superheated steam for drying foods has advantages to both consumers and industry as detailed by many researchers (Lane and Stern, 1956; Shibata and Mujumdar, 1994; Tang and Cenkowski, 2000; Deventer and Heijmans, 2001; Soponronnarit et al., 2006):

1. Use of superheated steam as the drying medium leads to an oxygen-free drying system, which prevents oxidative reactions, resulting in an improvement of the product quality.
2. SSD allows pasteurization, sterilization, and deodorization of food products during drying. In addition, products are partially cooked, with possible favorable changes in their textural properties.
3. SSD may reduce processing time and processing steps. For example, in producing parboiled rice by a conventional process, the process consists of three main stages, namely, soaking, steaming, and drying. However, steaming and drying can be combined into one stage with the use of SSD, thereby allowing a significantly shorter processing time.
4. Higher drying rates are obvious in both constant and falling rate periods if the product can be dried at a temperature above the inversion temperature since the temperature difference between particle and fluid stream is larger in superheated steam than in hot air, resulting in higher heat flux from the gas to the particle surface. More details about the inversion temperature will be given in Section 10.3. The higher drying rates would increase the dryer performance, which leads to a reduction in equipment size or an increase in drying capacity.
5. SSD may have high thermal efficiency if the exhaust steam can be used elsewhere in the process.
6. SSD enhances physical food qualities as it leads to less shrinkage and high product porosity due to evolution of moisture inside the product during drying.

However, SSD also has the following limitations:

1. There is unavoidable condensation at the beginning of drying because raw materials are generally fed into the system at ambient temperature. This results in an increase in the moisture content of materials by approximately 2%–3%, resulting in an increase in the drying time by 10%–15%. In addition to the increase in the moisture content, condensation may interrupt the drying system, particularly in the case of a fluidized-bed dryer. Condensation of steam causes particle surface to be very wet and hence the particles would

agglomerate, resulting in more difficulty in fluidizing them. To alleviate this problem, raw materials need to be warmed up before being fed into the dryer.
2. An SSD system is more complicated and requires higher investment for insulation and auxiliary heating than in the case of a hot-air drying system. Shut down and start up also take longer for a superheated-steam dryer than for a hot-air dryer.
3. Application of SSD for heat-sensitive materials is unfavorable. Products that may suffer degradation at higher temperatures cannot be dried in superheated steam. However, it may be possible to use a two-stage drying technique, i.e., SSD followed by hot-air drying to alleviate this shortcoming. For example, drying of chicken meat using this two-stage technique appears to produce a higher quality dried product, i.e., product with less brown color and higher rehydration ability (Nathakaranakule et al., 2007).

10.3 FUNDAMENTALS OF DRYING IN SUPERHEATED STEAM

During drying, moisture from a drying product vaporizes into the drying medium, which then carries the water vapor away. The drying rate remains constant as long as the evaporated moisture of the material is available at its surface. During this constant drying rate period, heat transfer controls the moisture evaporation rate. In the case of hot-air drying, the moisture evaporation rate can be calculated by:

$$\frac{dM_w}{dt} = \frac{hA\left(T_{\text{drying medium}} - T_{\text{samp sur}}\right)}{\Delta H_w^{\text{vap}}} \tag{10.1}$$

where

dM_w/dt is the drying rate (kg water s^{-1})
h is the heat transfer coefficient (W m^{-1}·K^{-1})
A is the surface area of material in contact with the drying medium (m^2)
ΔH_w^{vap} is the latent heat of evaporation of moisture (J kg^{-1})
T is the temperature (K)

The temperature at sample surface is equal to the wet bulb temperature of hot air. However, when hot air is replaced by superheated steam, $T_{\text{samp sur}}$ in Equation 10.1 is replaced by the saturation (boiling) temperature of steam at the dryer operating pressure. Equation 10.1 is derived based on the assumptions that other modes of heat transfer from the gas medium to the solid sample, such as sensible heat effects and heat losses from solid sample, are neglected.

According to Equation 10.1, the evaporation rate of moisture into superheated steam and hot air may have different values, depending on the temperature difference between the sample surface and the bulk gas/vapor phase, and on the heat transfer coefficient of the drying medium. When the drying temperature is lower than the so-called inversion temperature, the evaporation rate of moisture into hot air is higher than that into superheated steam as illustrated in Figure 10.2. On the other hand, the moisture evaporation rate into a superheated-steam environment becomes

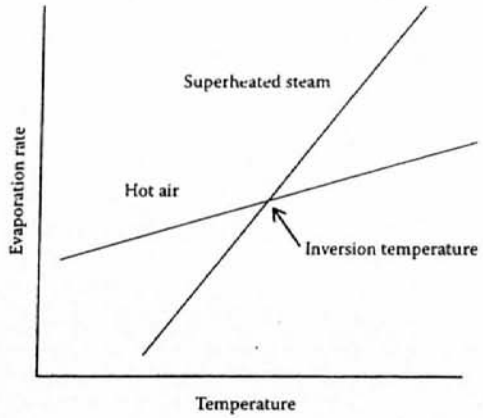

FIGURE 10.2 Variation of the evaporation rates with drying temperatures.

higher than that associated with a hot-air environment at temperatures beyond the inversion temperature.

Below the inversion temperature, the higher moisture evaporation rate in hot-air drying is related to the heat-transfer coefficient and the temperature difference between the sample surface and bulk gas phase. Considered at the same drying condition, i.e., a given gas velocity and a fixed operating pressure, both the heat-transfer coefficient and the temperature difference are higher for hot air than for superheated steam, being the latter variable more important. When the drying temperature reaches the inversion value, the temperature difference in Equation 10.1 is, in turn, smaller in hot-air drying than in SSD. However, this result can be compensated by the higher heat transfer coefficient for hot-air dying, and, hence, the drying rates in SSD and hot-air drying are equal at the inversion temperature. From this point on, the temperature difference is significantly larger for SSD. Moreover, the larger temperature difference in SSD is more dominant than the heat-transfer coefficient in hot-air drying. Thus, it provides higher heat flux and subsequently higher moisture evaporation rate in SSD.

The first experimental investigation to explore the inversion phenomenon was carried out by Yoshida and Hyōdō (1970). They reported an inversion temperature between 160°C and 176°C for the water–air countercurrent flow in a wetted-wall column. Chow and Chung (1983a,b) later presented numerical results of the evaporation of water into superheated steam and dry air for laminar (Chow and Chung, 1983a) and turbulent (Chow and Chung, 1983b) forced convection over a flat plate. Their analysis showed an inversion temperature of 250°C for laminar flow and 190°C for turbulent flow. Schwartze and Bröcker (2002) theoretically studied the evaporation of water into superheated steam, dry air, and humid air. They found the inversion temperature of 199°C for turbulent flow in a wetted-wall column.

The above findings are the results of evaporation rate, which is governed by convective transport phenomena. Several reports have shown that the inversion

temperature was also found in the case of porous food drying, in which internal moisture movement mainly governs overall transport mechanisms. The inversion temperature in this case varies from material to material. Prachayawarakorn et al. (2002), for example, dried shrimp in superheated steam and hot air and found the inversion temperature to be between 140°C and 150°C. For drying of potato slices, however, there existed an inversion temperature between 145°C and 160°C for the first drying stage, in which the moisture content was above 2.6 dry basis (d.b.) and between 125°C and 145°C during the last drying stage, when the moisture content was below 2.6 d.b. (Tang and Cenkowski, 2000).

10.3.1 Drying Characteristic Curves

During air-drying, the moisture content of the material decreases continually with time. An illustrative example of this phenomenon is shown in Figure 10.3. With superheated steam, however, the drying characteristic curve is different from that found with hot air; there is a gain in the moisture content in the early stage of drying. This increase in the moisture content is caused by the condensation of steam. However, for longer drying times, the drying curve becomes similar to the one in hot air.

Condensation occurs when superheated steam contacts the material surface, which is at a lower temperature. As a result, superheated steam releases its energy and changes its phase from vapor to liquid. The amount of steam condensed depends on the degree of superheat, which is defined as the difference between the actual

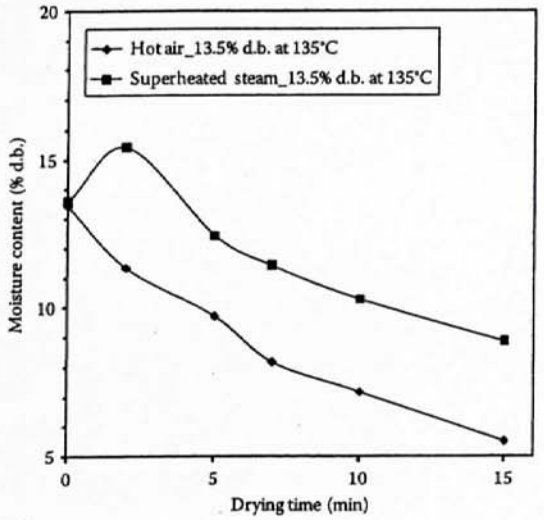

FIGURE 10.3 Drying curves of soybean in superheated-steam and hot-air fluidized bed. (From Prachayawarakorn, S. et al., *LWT-Food Sci. Technol.*, 39, 773, 2006. With permission.)

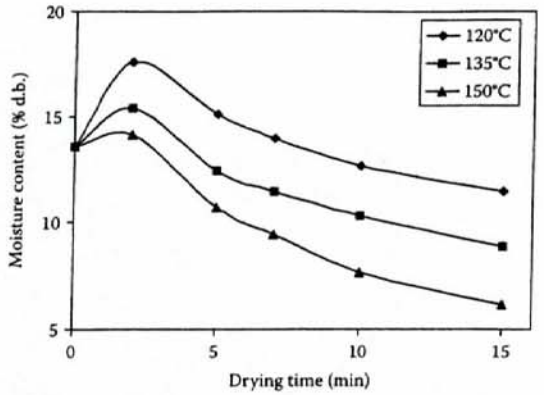

FIGURE 10.4 Change of moisture content of soybean at three different inlet steam temperatures. (From Prachayawarakorn, S. et al., *Drying Technol.*, 22, 2105, 2004. With permission.)

superheated-steam temperature and its saturation value at the dryer operating pressure. A higher degree of superheat obviously leads to a smaller amount of steam condensation, and thus to a smaller increase in the moisture content of the material. The effect of the degree of superheat on the moisture uptake can be seen in Figure 10.4.

Condensation of steam may render the dryer operation unstable, particularly in the case of a fluidized-bed dryer. Condensation and formation of liquid around the feed stream of food material leads to a difficulty in maintaining a desired level of fluidization. In such cases, solid preheating may be a useful option because the amount of steam condensation would then decrease.

Nevertheless, steam condensation does not have only the disadvantages as mentioned earlier. Actually, it sometimes provides several advantages. James et al. (2000) compared three different treatment methods for decontaminating lamb carcasses, namely, steam condensation, hot-water immersion, and chlorinated-hot-water immersion. All three treatments significantly reduced aerobic plate counts on the carcasses. There was no significant difference between steam and hot-water treatments; both treatments reduced the counts by approximately 1 $\log_{10}$ CFU cm^{-2}. In all cases, no significant differences were found in the evaluation of lean appearance, color appearance, odor, and overall acceptability of treated and untreated carcasses after 48 h of chilling and chilled storage. However, the use of steam seemed to have the greatest potential for industrial application since legislation and consumer concern would limit the use of chemical substances such as chlorine in decontamination applications, whereas the use of hot water may present problems in filtering, cleaning, and disposal stages.

In addition, steam condensation helps with gelatinization of starch. It has been reported that gelatinization of many starches is more complete in superheated steam than in hot air, in particular on the material surface, from which the moisture can easily be removed. Figure 10.5, for instance, shows morphologies of durian slices dried with superheated steam and hot air at 150°C (Jamradloedluk et al., 2007).

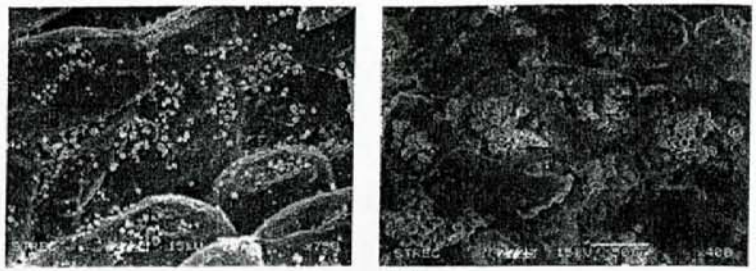

(a) (b)

(c)

FIGURE 10.5 Scanning electron micrographs of durian. (a) Surface of raw sample. (b) Surface of sample dried with hot air. (c) Surface of sample dried with superheated steam. (From Jamradloedluk, J. et al., *J. Food Eng.*, 78, 203, 2007. With permission.)

As shown in Figure 10.5a, durian starch granules are spherical with an average diameter of 1–3 μm. When the samples were dried with superheated steam, the starch granules disappeared as shown in Figure 10.5c, indicating that starch was gelatinized. In contrast, ungelatinized starch granules still appeared when durian was subjected to hot-air drying as shown in Figure 10.5b. The gelatinization of starch granules on the material surface led to a smoother surface, produced a transparent layer, and provided a glossy product.

10.3.2 Moisture Diffusivity

Moisture diffusivity is a fundamental parameter for analyzing, designing, and optimizing a drying system. When a material is being dried with hot air, moisture inside it moves through interfacial void spaces, evaporating and reaching the surface. Moisture is then transported away to the flowing stream on account of the moisture concentration difference between the thin, air boundary layer on the material surface and the bulk air stream. Inside the material, the transport of moisture in the falling rate period may occur by several mass transfer mechanisms, such as Knudsen diffusion, molecular diffusion, and capillary flow. All the drying mechanisms, as well as the effect of the porous structure of the solid material, are lumped together into an effective (apparent) diffusion coefficient. This effective moisture diffusivity can be determined from an experimental drying curve under a constant drying temperature, using classical analytical solutions of the diffusion equation, given by Crank (1975).

In SSD, the transport of moisture is driven by the pressure difference between the material surface and bulk stream and there is no mass transfer resistance on the gas side. During drying, the pressure at the material surface is equal to the saturation pressure at material temperature, and the pressure in the bulk stream is equal to the operating pressure. Moisture that exists inside the material starts to be removed when the material temperature reaches the saturation temperature of steam. The mechanisms of moisture movement inside the material in SSD are possibly similar to those in hot-air drying as mentioned above.

The morphology of the food material undergoing SSD may also be different from that of the material undergoing hot-air drying. Differences in such morphologies, in turn, affect the effective moisture diffusivity. Figure 10.6 shows experimental values and trends of the effective moisture diffusivity for foods dried by superheated steam and hot air, indicating lower values of this parameter when superheated steam is used (Poomsa-ad et al., 2002; Taechapairoj et al., 2004; Uengkimbuan et al., 2006; Jamradloedluk et al., 2007). The lower moisture diffusivity is due to the physically dense structures of food materials created during SSD. This led consequently to a lower drying rate in superheated steam compared to hot air.

10.3.3 Mathematical Modeling

This section describes a mathematical model that can be used to predict the temperature and moisture content of a material, especially cereal grain, in a batch superheated-steam dryer, operating near the atmospheric pressure. The model is first derived based on the fundamental transport equations for a drying particle, together with energy and mass balances for the dryer (fluidized bed), neglecting heat transfer by radiation, particle shape or size deformation (disregarding particle shrinkage or growth), and temperature gradients inside the particle. Superheated steam is injected into the bed of particles at constant inlet conditions (i.e., temperature, pressure, and mass flow rate). It is assumed that the inlet steam mass flow rate insures the bed-fluidization regime, and also that bubble formation and flow do not directly affect drying operation in SSD as they do in hot-air fluidized-bed dryers. Note that the free-bubbling regime assures a well mixing of superheated steam, but bubbles pass through the bed as an inactive phase, without the establishment of any concentration gradient to bring about water vapor transport, contrary to what occurs in hot-air drying. During drying, the wet particle with initially low temperature comes into contact with superheated steam. This naturally leads to steam condensation and an increase in both the particle moisture content and temperature. This initial condensation period is described in the mathematical model as the heating-up period. After the particle temperature reaches the saturation temperature of 100°C at an atmospheric pressure, condensation stops. Once the period of initial condensation is over, moisture evaporation starts. During the evaporation period, drying is presumably divided into two subperiods: constant drying-rate period and falling rate periods.

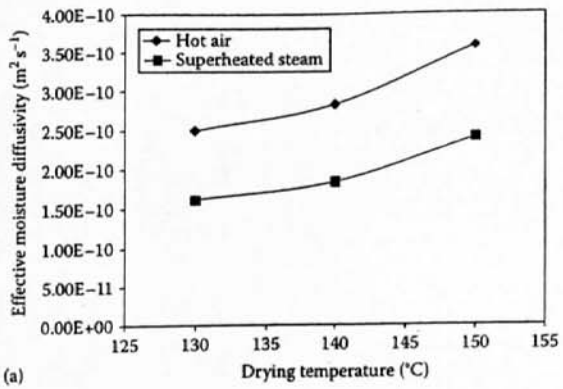

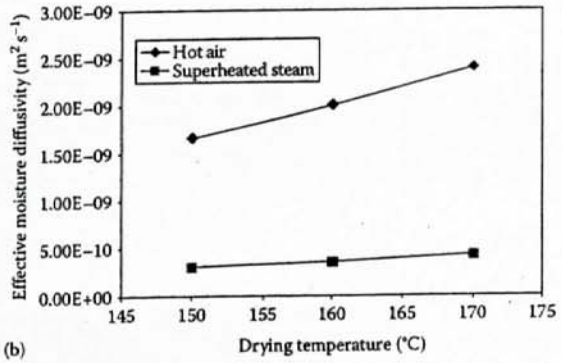

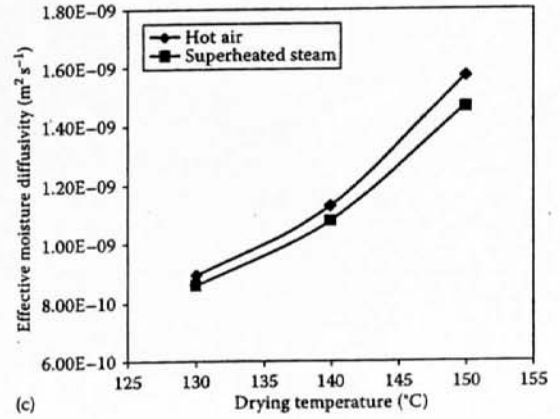

FIGURE 10.6 Comparison of effective moisture diffusivities of food materials dried with superheated steam and hot air. (a) Durian slice. (From Jamradloedluk, J. et al., *J. Food Eng.*, 78, 201, 2007. With permission.) (b) Rice. (From Taechapairoj, C. et al., *Drying Technol.*, 22, 729, 2004; and Poomsa-ad, N. et al., *Drying Technol.* 20, 202, 2002. With permission.) (c) Pork slice. (From Uengkimbuan, A. et al., *Drying Technol.* 24, 1666, 2004. With permission.)

10.3.3.1 Heating-Up Period

During the heating-up period, it is assumed that the condensed water forms a layer of liquid uniformly distributed over the entire external surface of each particle in the bed. This layer acts as a resistance to heat transfer from steam to particle surface. The rate of heat transfer, q, to particles into the bed can be described by:

$$q = h_{fl} A_{pfl\text{-}bed} \left(T_{st}^{sat} - T_p\right) \tag{10.2}$$

with $A_{pfl\text{-}bed}$ representing the total heat transfer area of particles into the bed, including the thickness of the liquid film covering them.

This rate of heat transfer is equal to the rate of heat released by steam plus the cooling of the condensate, which is expressed by (Holman, 1997):

$$q = \dot{M}_{cond} \left\{ c_{p,st} \left(T_{st}|_{in} - T_{st}^{sat}\right) + \Delta H^{vap} + \frac{3}{8} c_{p,w} \left(T_{st}^{sat} - T_p\right) \right\} \tag{10.3}$$

or

$$q = \dot{M}_{cond} \, \Delta H^{vap} \tag{10.4}$$

Equation 10.3 is obtained by assuming a linear temperature distribution in the condensed liquid film and a laminar flow of the liquid film. It is also assumed that, in the bed, the condensed water in contact with particles has their temperature. The condensation of steam onto a spherical particle is schematically shown in Figure 10.7.

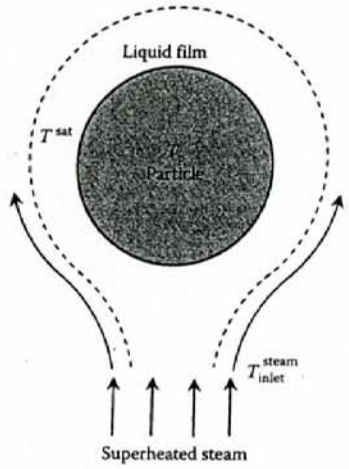

FIGURE 10.7 Liquid film condensation onto the surface of a particle.

Thus, based on these assumptions, the condensation rate of steam, $\dot{M}_{cond}$, can be calculated. The value of $\dot{M}_{cond}$ calculated with Equation 10.3 may not be precisely accurate since the thin liquid film may not be stagnated in reference to the fluidized particles and there are strong interactions amongst the solid particles, resulting in less uniformity of liquid film covering the entire particle surface. When the condensation rate is higher than the mass flow rate of steam entering the bed, one would expect that the steam flowing through the bed be completely condensed. In this case, the warming up of particles can be calculated using Equation 10.3, with $\dot{M}_{cond}$ replaced by the mass flow rate of steam. This situation may occur if the temperature of particles that are fed into the fluidized-bed dryer is rather low. Hence, the particles in the bed cannot fluidize.

For an energy balance of the solid phase, heat released from steam condensation can warm up both the particles and the condensed water, thus:

$$q = \left[M_{ss}\left(c_{p,s} + \bar{m}\, c_{p,w}\right) + M_{flw} c_{p,w}\right]\frac{dT_p}{dt} \tag{10.5}$$

where

c_p is the specific heat capacity
$\bar{m}$ is the average moisture content of particles
M_{flw} is the mass of condensed water covering the particle surface

The initial condition for solving Equation 10.5 is the particle temperature being equal to the ambient air temperature.

The heat transfer coefficient of the film condensation can be calculated from an empirical equation for an isolated sphere (Holman, 1997):

$$h_{fl} = 0.815\left[\frac{\rho_w(\rho_w - \rho_{st})g\Delta H^{vap}\lambda_{st}^3}{\mu_{st} d_p\left(T_{st}^{sat} - T_p\right)}\right]^{\frac{1}{4}} \tag{10.6}$$

The physical properties of steam and of condensed water are evaluated at the film temperature, $T_{fl} = \frac{T_{st}^{sat} + T_p}{2}$. Using Equation 10.6 to calculate the condensation heat transfer coefficient in the fluidized bed may lead to some errors since the fluidized particles change the gas fluid dynamics and subsequently the formation of boundary layers around the particles, which are not similar to the boundary layer around a single sphere.

The resulting steam condensation in the bed increases the moisture content of the particles, and this can be mathematically described by a differential mass balance for moisture in the particle. Assuming the food particle to be spherical with a constant volume, and neglecting convective effects, this mass balance (in spherical coordinates) is then expressed by

$$\frac{\partial m}{\partial t} = D_m^{eff}\left[\frac{\partial^2 m}{\partial r^2} + \frac{2}{r}\frac{\partial m}{\partial r}\right] \tag{10.7}$$

where D_m^{eff} is the effective diffusion coefficient ($m^2 s^{-1}$), assumed to be independent of the particle moisture content and temperature dependent. The value of D_m^{eff} during sorption of condensed water can be determined directly from soaking experiments at a given temperature. Initial and boundary conditions associated with Equation 10.7 are given by

$$m(r,t) = m_0, \quad \text{at } t = 0 \tag{10.8}$$

$$\left.\frac{\partial m}{\partial r}\right|_{r=0} = 0, \quad \text{at } t > 0 \tag{10.9}$$

$$m\left(\frac{d_p}{2}, t\right) = m_{eq,c} \quad \text{at } t > 0 \tag{10.10}$$

Equations 10.9 and 10.10 imply, respectively, that the minimum moisture content is at the center of the particle and that the surface moisture of the particle is in equilibrium with the condensed water. $m_{eq,c}$ is the moisture content at the particle surface, which is supposed to equilibrate with the condensed water covering the surface. The value of $m_{eq,c}$ can be determined by soaking the particles in hot water at the boiling-point temperatures until the particle mass does not change. The average moisture content of the particle, $\bar{m}$, is given by

$$\bar{m}(t) = \frac{4\pi}{V_p}\int_0^{d_p/2} m(r,t) r^2 dr \tag{10.11}$$

where V_p is the particle volume (m^3). The amount of the condensed water sorbed by all particles in the bed at time t, $M_{sor}(t)$, is

$$M_{sor}(t) = M_{ss}\left[\bar{m}(t) - \bar{m}(t - \Delta t)\right] \tag{10.12}$$

where the time interval, Δt, should be infinitesimal (i.e., tends to zero).

The amount of the remaining condensate in the bed at time t, M_{flw}, is thus:

$$M_{flw}(t) = \sum_{i=0}^{t}\left(\dot{M}_{cond}(i)\Delta t - M_{sor}(i)\right) \tag{10.13a}$$

Initial condensation of steam enables faster development of particle temperature. However, subsequent condensation rate decreases, whereas the rate of water, sorbed by particles, increases. These opposite behavior might result in the sorption rate being faster than the condensation rate. If such a case occurs, the gain in moisture by particles would come from the water condensation at the present time plus the remaining condensed water on the particle surface, resulting in a smaller amount of condensed water into the bed. In this case, the remaining water at the present time is calculated by Equation 10.13a, which can be rewritten as

$$M_{flw}(t) = \dot{M}_{cond}(t)\Delta t - M_{sor}(t) + \sum_{i=0}^{t-\Delta t} M_{flw}(i) \tag{10.13b}$$

As there is no available condensed water left at the particle surface before condensation stopped, the increase in moisture content cannot be calculated directly by Equation 10.7. Therefore, at this time t_H (time just before condensation stop), $M_{flw}(t_H) = 0$, $T_p(t_H) = T_{st}^{sat}$, and $M_{sor}(t) = M_{ss}\left[\bar{m}(t_H) - \bar{m}(t_H - \Delta t)\right]$. Then, upon dividing Equation 10.13b by M_{ss} and using these equations at $t = t_H$, one obtains:

$$\bar{m}(t_H) = \bar{m}(t_H - \Delta t) + \frac{\dot{M}_{cond}(t_H)\Delta t}{M_{ss}} + \sum_{i=0}^{t_{cond}-\Delta t} \frac{M_{flw}(i)}{M_{ss}} \tag{10.14}$$

From Equation 10.14, one may expect the occurrence of the constant drying rate period when the average particle moisture content is higher than the critical moisture content. Accordingly, the drying period should be divided into two: constant drying rate and the falling rate.

10.3.3.2 Drying Period

A mathematical description of the temperature changes of steam and particles within the bed is derived from an energy balance in the solid and gas phases. The solid-phase energy balance can generally be written as

$$hA_{p-bed}\left(T_{st}|_{bed} - T_p\right) = \left(-M_{ss}\frac{d\bar{m}}{dt}\right)\left[\Delta H^{vap} + c_{p,st}\left(T_{st}|_{bed} - T_p\right)\right] + M_{ss}\left(c_{p,s} + \bar{m}\,c_{p,w}\right)\frac{dT_p}{dt} \tag{10.15}$$

Equation 10.15 represents the energy used for vaporizing water and heating up this vapor to the steam temperature inside the bed, $T_{st|bed}$, (indicating that the steam within the bed is in a gaseous state), as well as for heating up the bed particles. When the particle temperature reaches the steam saturation value and drying starts in the constant rate regime, the last term on the right hand side of Equation 10.15 is neglected. However, this term is relevant for the falling rate period.

As observed from the experiments carried out in a fluidized bed (Soponronnarit et al., 2006), while the material is being dried, the temperature of steam inside the bed dryer, $T_{st}|_{bed}$, is lower than the one at the inlet, $T_{st}|_{in}$, but $T_{st}|_{bed}$ is insignificantly different from the exhaust steam temperature, $T_{st}|_{out}$. Therefore, at least for shallow fluidized-bed dryers, the gas phase can be considered to flow in perfect mixing inside the dryer chamber (i.e., $T_{st}|_{bed} = T_{st}|_{out}$), with its energy balance written as

$$\dot{M}_{st,in}\,c_{p,st}\left(T_{st}|_{in} - T_{ref}\right) - \dot{M}_{st,out}\,c_{p,st}\left(T_{st}|_{bed} - T_{ref}\right) = hA_{p-bed}\left(T_{st}|_{bed} - T_p\right) + \Gamma_{st-amb}A_{wall}\left(T_{st}|_{bed} - T_{amb}\right) \tag{10.16}$$

The first and second terms on the left-hand side of Equation 10.16 represent the energy carried by steam that, respectively, enters and leaves the drying chamber. This energy change is equivalent to the heat supplied for drying and heating particles plus the heat lost to the environment, whose temperature, T_{amb}, is known. In Equation 10.16, $\Gamma_{st\text{-}amb}$ represents the overall heat transfer coefficient between the steam inside the dryer and the surroundings, and A_{wall} is the contact area between the dryer walls and the surroundings, adopted as reference in the calculation of $\Gamma_{st\text{-}amb}$. It is assumed that the dryer internal wall is only in contact with steam, and particles therefore cannot lose their energy directly to the surroundings.

The gas-phase mass balance is now considered. The mass flow rate of steam leaving the drying chamber at any instant, $\dot{M}_{st,out}$, can be calculated by

$$\dot{M}_{st,out} = \dot{M}_{st,in} + \left(-M_{ss}\frac{d\bar{m}}{dt}\right) \tag{10.17}$$

Equation 10.17 represents an evaporation operation ($d\bar{m}/dt < 0$) leading to the mass flow rate of steam at the outlet being higher than that at the inlet under normal operation. Condensation, on the other hand, decreases the steam mass flow rate within the bed ($d\bar{m}/dt > 0$).

10.3.3.2.1 Constant-Rate Drying Period

As mentioned earlier, when the period of condensation finishes, the particle temperature reaches the steam saturation temperature ($T_p = T_{st}^{sat}$) and drying starts with the evaporation of unbound water from particle. Since only free water is removed in this case, drying occurs at a constant rate dictated by external conditions (steam flow rate, temperature, and pressure). This constant-rate drying period can be divided into two subperiods: the first one concerning the evaporation of the condensed water film covering particles, and the second one regarding the unbound water on the surface of particles.

During the first subperiod, one can consider that the interface at which water evaporates moves with decreasing film thickness until reaching the particle surface. Therefore, the moisture profile inside the particle remains unchanged until all condensed water has been removed from the surface. The temperatures of both the particle and the condensed water remain equal to T_{st}^{sat} and Equation 10.15 is reduced to

$$h_{fl}A_{pfl-bed}\left(T_{st}|_{bed} - T_{st}^{sat}\right) = \left(-\frac{dM_{flw}}{dt}\right)\left[\Delta H^{vap} + c_{p,st}\left(T_{st}|_{bed} - T_{st}^{sat}\right)\right] \tag{10.18a}$$

After the condensed water film has been removed, unbound water starts to be evaporated at particle surface, which marks the beginning of the second drying subperiod. In this case, Equation 10.18a is changed to Equation 10.18b:

$$hA_{p-bed}\left(T_{st}|_{bed} - T_{st}^{sat}\right) = \left(-M_{ss}\frac{d\bar{m}}{dt}\right)\left[\Delta H^{vap} + c_{p,st}\left(T_{st}|_{bed} - T_{st}^{sat}\right)\right] \tag{10.18b}$$

where h, the heat transfer coefficient between particle and steam, is determined from Ranz and Marshall (1952). The changes in internal moisture content of particle, and therefore the vaporization rate, can be calculated using Equation 10.7, with the following initial and boundary conditions:

$$m(r,t) = m(r,t_1), \quad \text{at } t = t_1 \tag{10.19}$$

$$\left.\frac{\partial m}{\partial r}\right|_{r=0} = 0, \quad \text{at } t > t_1 \tag{10.20}$$

$$-\frac{6D_m^{eff}}{d_p}\left.\frac{\partial m}{\partial r}\right|_{r=\frac{d_p}{2}} = N_c, \quad \text{at } t > t_1 \tag{10.21}$$

where

t_1 is the time at the end of condensed water removal period (s)

N_c is the constant drying rate (kg evaporated water/s·kg dry matter), which can be determined experimentally

Equation 10.19 represents the existing moisture gradients at the beginning of the second subperiod of constant-rate drying. As mentioned earlier, this moisture profile inside the particle is the one obtained at the end of the condensed water removal period, since during the first subperiod of constant-rate drying only the condensed water film covering the particle is removed.

For both subperiods, the energy balance for the gas phase (steam) is still similar to Equation 10.16, with T_p replaced by T_{ti}^{sat}.

10.3.3.2.2 Falling-Rate Drying Period

After the moisture content of the particle drops below the critical moisture content, further reduction of moisture occurs in the falling-rate drying period. The critical moisture content of the particle can be determined from the experiment and this value is an input parameter in the model. Equation 10.7 still describes water diffusion inside particle, now with the following initial and boundary conditions:

$$m(r,t) = m(r,t_2), \quad \text{at } t = t_2 \tag{10.22}$$

$$\left.\frac{\partial m}{\partial r}\right|_{r=0} = 0, \quad \text{at } t > t_2 \tag{10.23}$$

$$m\left(\frac{d_p}{2},t\right) = m_{eq}, \quad \text{at } t > t_2 \tag{10.24}$$

where

t_2 is the drying time at the end of the constant-rate drying period (s)

m_{eq} is the equilibrium moisture content, whose value is the moisture content of the particle in equilibrium with superheated steam at a given temperature and pressure

In SSD near the atmospheric pressure, the value of m_{eq} is assumed to be zero since the high drying temperature of 100°C is used The calculations of the steam bed temperature. the particle temperature, and the steam flow still follow Equations 10.15 through 10.17, with the particle temperature increasing with time from the steam saturation temperature to one close to the steam bed temperature ($=T_{si}|_{out}$).

In Figure 10.8, the predicted and experimental data of moisture content vs. time for drying paddy in a superheated-steam fluidized-bed dryer at 150°C are compared. These results show that the prediction of the time evolution of the paddy moisture content from the mathematical model presented is very closed to experimental data. The calculations also indicated that the period of steam condensation in the bed of particles being fluidized depends on the steam velocity, being shorter at higher steam velocities. More specifically, the condensation periods were around 2–2.5 s for the steam velocities of 1.3 and 1.5 u_{mf} (corresponding to the superficial velocities of 2.6–3 m/s). For the thin layer dryer, in which superheated steam flows across material and the material is not fluidized, condensation takes longer than in the fluidized-bed dryer. Pronyk et al. (2004) investigated the drying characteristics of foodstuffs using a superheated-steam thin-layer dryer at velocities between 0.25 and 0.35 ms^{-1} and steam temperatures from 125°C to 165°C. It was found that the condensation time was in the range of 6–7 s for Asian noodle before drying started.

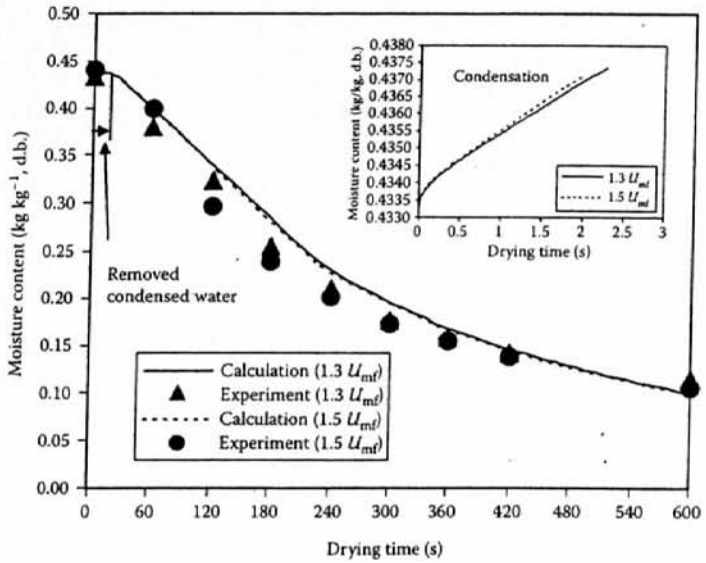

FIGURE 10.8 Comparison between predicted and experimental data of moisture content of paddy at superficial velocities of 1.3 and 1.5 times minimum fluidization velocity and inlet steam temperature of 150°C. (From Soponronnarit, S. et al., *Drying Technol.*, 24, 1462, 2006. With permission.)

10.4 APPLICATIONS OF SUPERHEATED STEAM DRYING TO FOOD MATERIALS

10.4.1 Parboiled Rice

Parboiled rice offers some advantages over unparboiled rice, such as strengthening of kernel integrity, high milling yield, and decrease in solid loss after cooking. Other characteristics of parboiled rice are its firmer and less sticky texture. A process for producing parboiled rice consists essentially of three steps including soaking of paddy, steaming, and drying to the predetermined moisture content. Figure 10.9 shows the conventional production process of parboiled rice that is currently operated in some countries. This process generally takes 3–4 h for the steps of soaking and drying to a moisture content of 22% d.b. A hot-air fluidized-bed dryer is used to dry paddy to moisture content of 39% d.b. (28.5% w.b.). Then, paddy is tempered (see No. 5) and dried again in a fluidized-bed dryer to 21% d.b.

Recently, however, Taechapairoj et al. (2004) found that drying of paddy in a superheated-steam fluidized bed could give a rice texture similar to the parboiled rice; milling yield was also noted to be higher. The moisture content of paddy after drying should not be lower than 18% d.b., otherwise the head rice yield would be very low. The kinetics of rice-starch gelatinization during SSD could suitably be explained by a zeroth-order reaction rate whose rate constant, N_k (s^{-1}), was related to the bed depth and drying temperature in the following form:

$$N_k = -3.0340\times10^{1} + 3.1920H_{bed} - 1.0984\times10^{-1}H_{bed}^2 - \exp\left(-\frac{1.5186\times10^{3}}{T}\right) \quad (10.25)$$

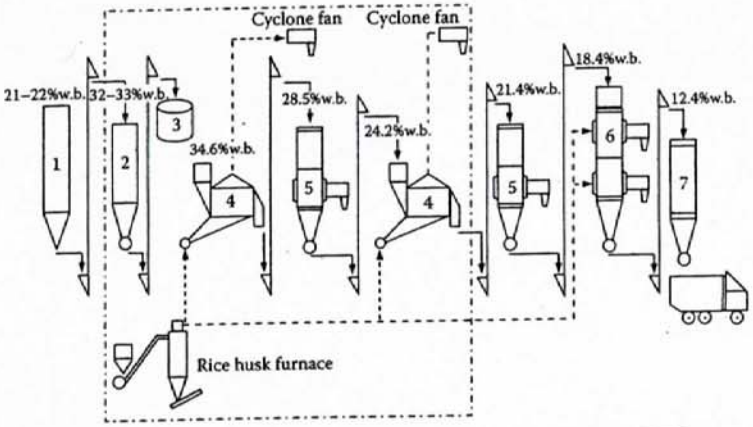

1. Soaking tank 2. Steamer 3. Ambient air ventilation 4. Fluidized bed dryer 5. Tempering and air ventilation 6. LSU dryer 7. Storage bin

FIGURE 10.9 Conventional parboiled rice process. (From Rordprapat, W. et al., *J. R. Inst. Thailand*, 30, 377, 2005. With permission.)

where
H_{bed} is the bed depth (cm)
T is the drying temperature (K)

The values of correlation coefficient and absolute mean error associated with Equation 10.25 were 0.97 and 3.66, respectively. Complete gelatinization of rice starch could be established within 5–6 min at steam temperatures of 150°C–160°C, and within 4 min at a steam temperature of 170°C.

The findings of parboiled rice characteristics in SSD would make a significant progress in the parboiling process because superheated steam itself can act as both steaming and drying media at the same time, thereby reducing steps in the parboiling process. With superheated steam, steaming and drying can be combined into one step. Thus, all the units from No. 2 to No. 5, shown in Figure 10.9 by the dash-dot line (Rordprapat et al., 2005), could be replaced by a single superheated-steam dryer. Additionally, the processing time would be much shorter.

Soponronnarit et al. (2006) successfully fabricated and tested a pilot-scale, continuous superheated-steam fluidized-bed dryer, with a capacity of 100 kg h^{-1}. A cyclonic rice husk furnace was used as a heating source to generate steam for the dryer. A schematic diagram of the referred pilot-scale dryer is shown in Figure 10.10.

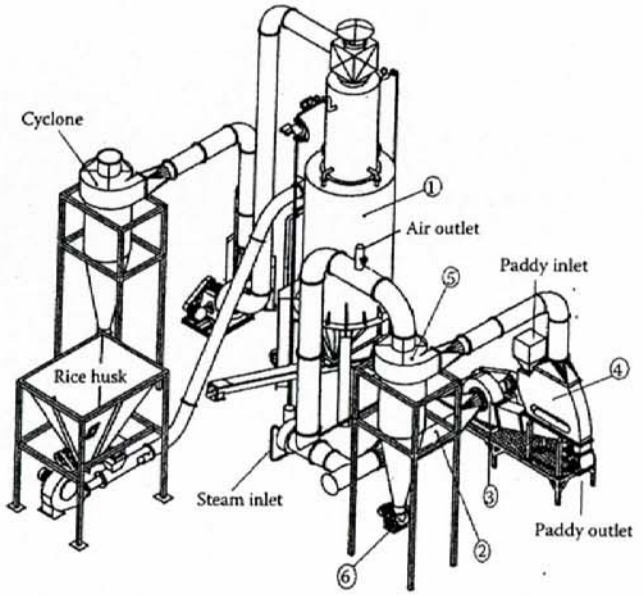

1. Bolier 2. Superheater 3. Blower 4. Drying chamber 5. Cyclone 6. Rotary value

FIGURE 10.10 Schematic diagram of a pilot-scale superheated-steam fluidized bed. (From Soponronnarit, S. et al., *Drying Technol.*, 24, 1462, 2006. With permission.)

TABLE 10.1
Paddy Qualities (Chainat 1 Variety) Soaked at 70°C for 7–8 h and Dried at Different Inlet Steam Temperatures

Drying Condition	Feed Rate ($kg\,h^{-1}$)	Moisture Content (d.b.)	Head Rice Yield (%)	Whiteness	White Belly (%)	Hardness (N)	Water Adsorption (g Water/g Rice)
After soaking	—	0.456 ± 0.008	56.6 ± 1.1[a]	39.0 ± 0.2[a]	5.7 ± 0.6*[a]	37.9 ± 1.3[a]	3.51 ± 0.07[a]
128°C	106	0.290 ± 0.008	63.5 ± 0.6[b]	32.2 ± 0.8[b]	0[b]	48.6 ± 0.9[b]	2.82 ± 0.05[b]
144°C	98	0.23 ± 0.004	66.9 ± 0.6[c]	29.4 ± 0.5[c]	0[b]	51.9 ± 0.6[c]	2.19 ± 0.01[c]
160°C	120	0.218 ± 0.004	67.9 ± 0.6[c]	28.0 ± 0.6[c]	0[b]	55.0 ± 1.3[d]	3.99 ± 0.05[d]

Source: Soponronnarit, S. et al., *Drying Technol.*, 24, 1462, 2006. With permission.
Note: Same letters on the same column indicate that values are insignificantly different at $p < 0.05$.
* Chalky grains.

The equipment was also installed in and demonstrated to some parboiled rice factories. Table 10.1 shows the paddy quality after drying with superheated steam. Before drying, paddy was soaked with hot water at 70°C for 7–8 h. The head rice yield of the reference paddy, which was dried in shade, was 56.6%, and the white belly, representing the incomplete gelatinization, was 5.6%. After drying, the head rice yield was improved, being in the range of 63%–68%, and the white belly was not observed. Moreover, the value of hardness of dried parboiled rice significantly increased while less water was adsorbed.

Figure 10.11 shows the pasting viscosity of rice flour after SSD. It can be seen that the peak viscosity, final viscosity, and setback viscosity of dried rice flour are lower than those of the reference rice flour. The lowering of setback viscosity implies a firmer texture of rice flour. The trend of changing pasting viscosity of rice flour dried in SSD was similar to that of commercial parboiled rice obtained from the conventional process, but the values themselves are lower. Note that the extent to which the viscosity of rice flour obtained from the superheated-steam treatment is lower depends on the drying temperature. The pasting curve of flour made from rice dried at a temperature of 128°C is comparable to that of the commercially produced parboiled rice flour.

10.4.2 Soybean Meal

Full-fat soybean or soybean prior to oil extraction is used as a feedstuff because of its high-oil and high-quality protein contents. However, the presence of biologically active compounds in raw full-fat soybean such as trypsin inhibitors, hemagglutinins,

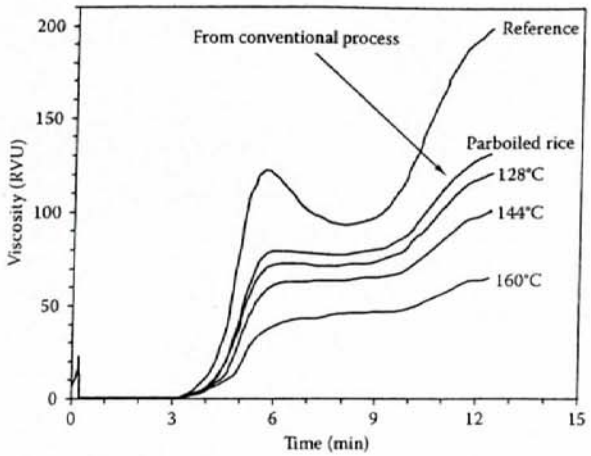

FIGURE 10.11 Pasting viscosities of rice flour samples dried at different steam temperatures. (From Soponronnarit, S. et al., *Drying Technol.*, 24, 1466, 2006. With permission.)

lectins, and saponins limits the utilization of its nutritive values (Hensen et al., 1987; Liener, 1994), resulting in compromised health and performance of nonruminants and immature ruminants. To eliminate these antinutritional factors, heat treatment is needed. Trypsin inhibitors are the main parameter used to control the quality of soybean meal. However, direct measurement of trypsin inhibitors is not frequently practiced. Instead, the urease activity is usually measured to indicate the activity of trypsin inhibitors because their inactivation rate is equal to that of the urease enzyme (Baker and Mustakas, 1973). The residual urease activity for adequately treated soybean is in the range of 10% and 20%; a value below 10% indicates overheating.

Heat-treatment methods frequently used are, for example, cooking, microwave, and roasting (Raghavan and Harper, 1974; Hensen et al., 1987; Stewart et al., 2003). Prachayawarakorn et al. (2006) studied the treatment of full-fat soybean using superheated steam and hot-air fluidized-bed dryers. It was found that both heating media could eliminate the urease enzyme, but at different rates, although the medium temperature used was the same. Insufficient inactivation was obvious with hot air at 120°C for soybean with initial moisture content of 13.5% d.b. As shown in Figure 10.12, the residual urease activity remained steadily at 40% although an extended drying period was applied. As the initial moisture content of soybean increased to 19.5% d.b., however, sufficient inactivation was noted at a heating time of over 25 min. In contrast to hot air, inactivation of the urease enzyme could be achieved at a superheated-steam temperature of 120°C; the levels of residual activity were below 20% for soybean with initial moisture contents of 13.5% and 19.5% d.b. when heated for 7 and 5 min, respectively. The thermal inactivation of urease followed a modified first-order reaction model, which is expressed by

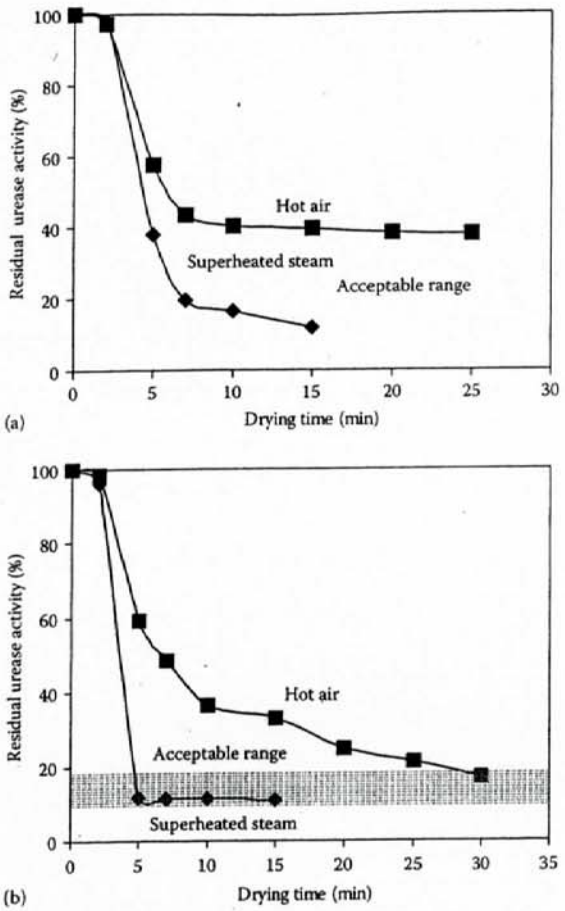

FIGURE 10.12 Apparent inactivation kinetics of urease inactivation present in soybean during thermal treatments with superheated steam and hot air at 120°C: (a) M_{in} = 13.5 % d.b. and (b) M_{in} = 19.5% d.b. (From Prachayawarakorn, S. et al., *LWT-Food Sci. Technol.*, 39, 775, 2006. With permission.)

$$\frac{a_{ur}(t) - a_{ur}|_{eq}}{a_{ur}|_{in} - a_{ur}|_{eq}} = \exp(-N_k t) \tag{10.26}$$

where

$a_{ur}(t)$ is the residual urease activity at time t (%)
$a_{ur}|_{in}$ is the urease activity at the beginning of heat treatment (%)
$a_{ur}|_{eq}$ is the residual urease activity at infinite time (%)
N_k is the apparent constant kinetic rate (min^{-1})
t is the drying time (min)

The apparent constant kinetic rate could be expressed as a function of the operating parameters, i.e., heating temperature and moisture content, as

$$N_k = \left[-1.01\times10^4 + 7.50\times10^{-2}T^2 - 7.66\times10^4 m_{in} + 1.89\times10^4 m_{in}^2 + \frac{2.62\times10^7 m_{in}}{T}\right] \times \exp\left(-\frac{5.35\times10^{-1}}{m_{in}} - \frac{1.51\times10^3}{T}\right) \tag{10.27}$$

In addition, the expression for $a_{ur}|_{eq}$ is given by

$$a_{ur}|_{eq} = \left(-4.7523\times10^{-2} + 7.1742\times10^{-2} m_{in}^2 + 1.2200\times10^{-4} T\right) \times \exp\left(\frac{3.2273\times10^3 - 9.7815\times10^2 m_{in}}{T}\right) \tag{10.28}$$

Equations 10.27 and 10.28 both presented a correlation coefficient equal to 0.95, and root mean square errors of 0.347 and 1.47, respectively.

Prachayawarakorn et al. (2006) recommended that a fluidized-bed dryer should be operated at 135°C–150°C for hot air and below 135°C for superheated steam to eliminate the urease enzyme present in soybean. This could simultaneously preserve the nutritional qualities, protein solubility, and lysine content. Under such temperature ranges, the use of superheated steam as the heating/drying medium resulted in higher protein solubility of treated sample than the use hot-air drying when applied to the dried soybean (13.5% d.b.), as can be seen in Table 10.2. In addition, the protein solubility of soybean was similar to that treated by an industrial micronizer (Wiriyaumpaiwong et al., 2004). For the moist soybean, the heating medium types did not affect the quality since the urease enzyme was inactivated over a short period of time before protein denaturation largely occurred.

10.4.3 Snack Foods

Snack foods, e.g., potato chips, banana chips, durian chips, are generally commercially produced by deep-fat frying. The development of a porous structure provides snacks with better quality, especially in terms of texture, compared with air-dried products. Snack products typically have a high oil content and cannot be kept for a long period of time due to possible lipid oxidation, leading to rancidity. In addition, consumers who are concerned with their health may dislike these products. The product with low fat content is an interesting commodity to the consumer.

High-temperature drying could be an alternative to frying to produce low-fat snack products. During high-temperature drying, the product moisture vaporizes and expands rapidly, thereby allowing the formation of pores. Li et al. (1999) studied superheated-steam-impingement drying of tortilla chips and founded that a higher steam temperature resulted in more pores, coarser appearance, and higher modulus of deformation of tortilla chips. In addition, the superheated steam-dried tortilla chips had fewer but

TABLE 10.2
Protein Solubility and Lysine Content of Soybean Treated with Superheated Steam and Hot Air at Various Temperatures

Temperature (°C)		m_{in} (% d.b.)	Heating Time (min)	$m(t)$ (% d.b.)	Urease Activity (%)	Protein Solubility (%)	Lysine Content (mg g^{-1} Soybean)
Raw soybean					100	94.28	2.9–3.1
Hot air	120	13.5	50	3.9	37	71.1	N/A
		19.5	30	6.9	19	70.98	3.0
	135	13.5	5	9.7	15	78.68	3.1
		19.5	5	14.4	13	84.33	N/A
	150	13.5	5	8.2	16	74.17	N/A
		19.5	2	15.5	10	87.86	N/A
Superheated steam	120	13.5	7	13.9	16	85.66	2.8
		19.5	5	18.3	12	85.2	2.7
	135	13.5	5	12.4	11	71.76	2.7
		19.5	5	16.5	9	82.25	2.7
	150	13.5	5	10.6	12	54.94	2.8
		19.5	2	18.9	11	83.84	N/A

Source: Prachayawarakorn, S. et al., *LWT-Food Sci. Technol.*, 39, 776, 2006. With permission.
N/A, not available.

larger pores than the air-dried product. Similar results were also found for dried durian chips (Jamradloedluk et al., 2007). In spite of the different morphologies of products obtained from the two drying media, textural properties such as hardness and stiffness were not significantly different. In the case of some particular fruits such as banana, however, though pores could be formed during high-temperature drying and the texture of the final product might be acceptable, the color of the product normally becomes brown when its moisture content is reduced below 80% d.b. (Prachayawarakorn et al., 2008). In addition, some pores might collapse during the early drying period, resulting in shrinkage of the product and subsequent less crispiness and hard texture. To avoid shrinkage, the structure should be rigid so that it can resist stresses generated during drying. This can be achieved by drying the product at temperatures below the glass transition temperature, and the freezing drying technique is normally applied.

Another technique that provides less material shrinkage involves puffing, by which the moisture inside the material is rapidly vaporized. Vapor expansion inside the product then creates voids or ruptures the existing structure, leading to a more porous dried product. Boualaphanh et al. (2008) studied the textural properties of banana after puffing with superheated steam at different conditions; their experimental results are shown in Figure 10.13, indicating that puffing temperature and moisture content of banana before puffing strongly affected the textural properties and shrinkage of the product. The sample shrunk least, approximately 10%–15%, when the moisture content of banana before puffing ranged between 20% and 25% d.b.

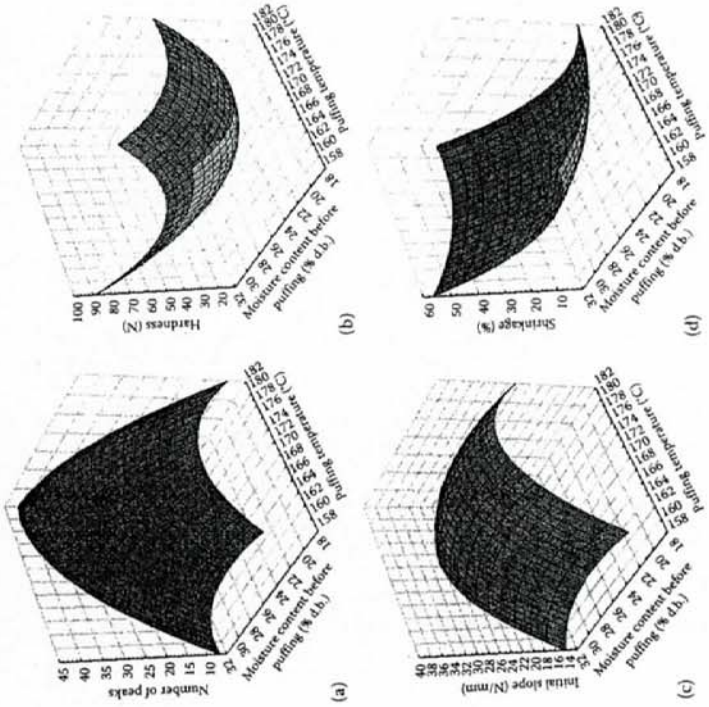

FIGURE 10.13 Quality attributes of banana puffed at different conditions (2 min puffing time). (a) Number of peaks. (b) Hardness. (c) Initial slope. (d) Shrinkage. (From Boualaphanh, K. et al., Optimization of the superheated steam puffing of banana, in *Proceedings of the 9th Thai Society of Agricultural Engineering Conference*, Chiang Mai, Thailand, January 31–February 1, 2008, CR2-16 [in Thai]. With permission.)

and the puffing temperature was in the range of 170°C–180°C. Under these puffing conditions, the color of the sample fell into the color group of grayed-orange 163C, and the textural property values were in ranges of 35 ± 5 N/mm for the initial slope, 37 ± 5 for the number of peaks and 33 ± 11 N for the hardness. These quality attributes were similar to those of the commercially vacuum fried product; the textural property values of the commercial product were 48 ± 8 N for the hardness, 42 ± 5 for the number of peaks and 45 ± 16 for the initial slope.

Figure 10.14 shows the morphology of puffed banana, indicating the very large voids within the banana sample and the small pores at the exterior. The produced large pores imply the vaporization and expansion of moisture during superheated-steam puffing.

However, a drawback of superheated steam became evident when it was applied to pop amaranth seeds (Iyota et al., 2005). Amaranth, a well-known product in the market as a source of food and high nutritional components, can be consumed after popping. The volume expansion after popping is an important parameter; a high volume expansion produces softer and more appealing texture. Figure 10.15 shows the volume expansion ratio of popped amaranth seeds at different temperatures. In hot air, the maximum expansion ratio reached 7.7 at 260°C. A decrease in expansion ratio and browning occurred at higher temperature of 290°C. In the case of superheated steam, the expansion ratio was approximately 10% lower than that obtained in hot air. This occurred because the seed coats were apparently softened by steam condensation.

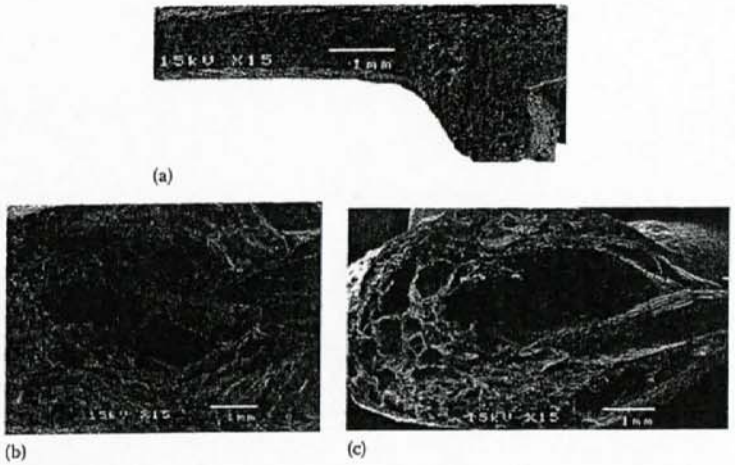

FIGURE 10.14 Morphologies of banana at different puffing temperatures. (a) No puffing. (b) Puffing temperature of 170°C. (c) Puffing temperature of 180°C. (From Boualaphanh, K. et al., Optimization of the superheated steam puffing of banana, in *Proceedings of the 9th Thai Society of Agricultural Engineering Conference*, Chiang Mai, Thailand, January 31–February 1, 2008, CR2-16 [in Thai]. With permission.)

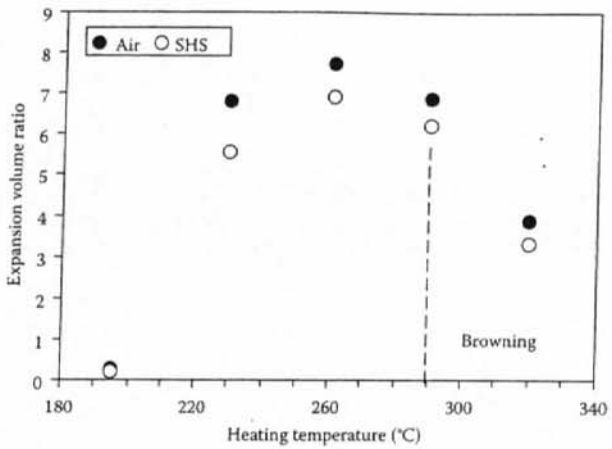

FIGURE 10.15 Effect of heating temperature on volume expansion ratio of amaranth seed in hot air and superheated steam (SHS) (initial moisture content of 13% d.b.). (From Iyota, H. et al., *Drying Technol.*, 23, 1287, 2005. With permission.)

10.5 CONCLUDING REMARKS

SSD is a feasible alternative to hot-air drying for a number of food products. The condensation of steam onto the material surface provides a rapid temperature rise, and this causes the food quality obtained from SSD to be different from that related to hot-air drying. The physical appearance of foods is better in SSD than in the hot-air drying, particularly when SSD is applied to starchy foods. Superheated-steam dried products such as tortilla, potato, and durian chips have a smoother surface and are glossier since the starch present in them can form a gel network to a larger extent in SSD than in the case of hot-air drying. Paddy dried by superheated steam has physicochemical and physical properties similar to those of parboiled rice. A temperature of 150°C is recommended for the dryer operation to produce parboiled rice.

In addition to the drying of starch-based foods, superheated steam can also be applied to eliminate the antinutritional factors present in legumes. However, the treatment of soybean with superheated steam should be done at temperatures below 135°C to preserve the protein solubility at the level that is required for feed meal.

A mathematical model for SSD that includes both steam condensation and drying has been derived based on the transport equations for drying a single particle, together with the energy and mass balances in the dryer. It can predict the change of moisture content of product during SSD relatively well. The mathematical model developed for the fluidized-bed dryer can be extended to other dryer types, with some modifications in the governing equations.

ACKNOWLEDGMENTS

The authors express their sincere appreciation to the Thailand Research Fund and Commission on Higher Education for the financial support of projects for more than 10 years.

REFERENCES

Baker, E.C. and Mustakas, G.C. 1973. Heat inactivation of trypsin inhibitor, lipoxgygenase and urease in soybeans: Effect of acid and base additives. *J. Am. Oil Chem. Soc.* 50:137–141.

Boualaphanh, K., Prachayawarakorn, S., and Soponronnarit, S. 2008. Optimization of the superheated steam puffing of banana. In *Proceedings of the 9th Thai Society of Agricultural Engineering Conference*. Chiang Mai, Thailand, January 31–February 1, 2008, CR2-16 (in Thai).

Chen, Z., Wu, W., and Agarwal, P.K. 2000. Steam-drying of coal. Part 1. Modeling the behavior of a single particle. *Fuel* 79:961–973.

Chow, L.C. and Chung, J.N. 1983a. Evaporation of water into a laminar stream of air and superheated steam. *Int. J. Heat Mass Transfer* 26:373–380.

Chow, L.C. and Chung, J.N. 1983b. Water evaporation into a turbulent stream of air, humid air or superheated steam. In *Proceedings of the ASME National Heat Transfer Conference*, No. 83-HT-2 ASME, New York.

Crank, J. 1975. *The Mathematics of Diffusion*, 2nd ed. Oxford, NY: Clarendon Press.

Deventer, H.C. and Heijmans R.M.H. 2001. Drying with superheated steam. *Drying Technol.* 19:2033–2045.

Douglas, W.J.M. 1994. Drying paper in superheated steam. *Drying Technol.* 12:1341–1355.

Hensen, B.C., Flores, E.S., Tanksley, Jr., T.D., and Knabe, D.A. 1987. Effect of different heat treatments during processing of soybean meal on nursery and growing pig performance. *J. Anim. Sci.* 65:1283–1291.

Holman, J.P. 1997. *Heat Transfer*, 8th ed. New York: McGraw-Hill.

Iyota, H., Konishi, Y., Inoue, T., Yoshida, K., Nishimura, N., and Nomura, T. 2005. Popping of amaranth seeds in hot air and superheated steam. *Drying Technol.* 23:1273–1287.

Iyota, H., Nishimura, N., Onuma, T., and Nomura, T. 2001. Drying of sliced raw potatoes in superheated steam and hot air. *Drying Technol.* 19:1411–1424.

James, C., Thornton, J.A., Ketteringham, L., and James, S.J. 2000. Effect of steam condensation, hot water or chlorinated hot water immersion on bacterial numbers and quality of lamb carcasses. *J. Food Eng.* 43:219–225.

Jamradloedluk, J., Nathakaranakule, A., Soponronnarit, S., and Prachayawarakorn, S. 2007. Influences of drying medium and temperature on drying kinetics and quality attributes of durian chip. *J. Food Eng.* 78:198–205.

Lane, A.M. and Stern, S. 1956. Application of superheated-vapor atmospheres to drying. *Mech. Eng.* 78:423–426.

Li, Y.B., Seyed-Yagoobi, J., Moreira, R.G., and Yamsaengsung, R. 1999. Superheated steam impingement drying of tortilla chips. *Drying Technol.* 17:191–213.

Liener, I.E. 1994. Implications of antinutritional components in soybean foods. *Crit. Rev. Food Sci. Nutr.* 34:31–67.

Markowski, M., Cenkowski, S., Hatcher, D.W., Dexter, J.E., and Edwards, N.M. 2003. The effect of superheated steam dehydration kinetics on textural properties of Asian noodles. *Trans. ASAE* 46:389–395.

Nathakaranakule, A., Kraiwanichkul, W., and Soponronnarit, S. 2007. Comparative study of different combined superheated steam drying techniques for chicken meat. *J. Food Eng.* 80:1023–1030.

Pang, S. and Dakin, M. 1999. Drying rate and temperature profile for superheated steam vacuum drying and moist air drying of softwood lumber. *Drying Technol.* 17:1135–1147.

Poomsa-ad, N., Soponronnarit, S., Prachayawarakorn, S., and Terdyothin, A. 2002. Effect of tempering on subsequent drying of paddy using fluidization. *Drying Technol.* 20:195–210.

Prachayawarakorn, S., Prachayawasin, P., and Soponronnarit, S. 2006. Heating process of soybean using hot-air and superheated-steam fluidized-bed dryer. *LWT-Food Sci. Technol.* 39:770–778.

Prachayawarakorn, S., Soponronnarit, S., Wetchacama, S., and Jaisut, D. 2002. Desorption isotherms and drying characteristics of shrimp in superheated steam and hot air. *Drying Technol.* 20:669–684.

Prachayawarakorn, S., Tia, W., Plyto, N., and Soponronnarit, S. 2008. Drying kinetics and quality attributes of low-fat banana slices dried at high temperature. *J. Food Eng.* 85:509–517.

Pronyk, C., Cenkowski, S., and Muir, W.E. 2004. Drying foodstuffs with superheated steam. *Drying Technol.* 22:899–916.

Raghavan, G.S.V. and Harper, J.M. 1974. Nutritive value of salt-bed roasted soybean for broiler chicks. *Poultry Sci.* 53:547–553.

Ranz, W. and Marshall, W. 1952. Evaporation from drops-Part I. *Chem. Eng. Prog.* 48, 141.

Rordprapat, W., Nathakaranakule, A., Tia, W., and Soponronnarit, S. 2005. Development of a superheated-steam-fluidized-bed dryer for parboiled rice. *J. R. Inst. Thailand.* 30:363–378 (in Thai).

Schwartze, J.P. and Bröcker, S. 2002. A theoretical explanation for the inversion temperature. *Chem. Eng. J.* 86:61–67.

Shibata, H. and Mujumdar, A.S. 1994. Steam drying technologies: Japanese R&D. *Drying Technol.* 12:1485–1524.

Soponronnarit, S., Prachayawarakorn, S., Rordprapat, W., Nathakaranakule, A., and Tia, W. 2006. A superheated-steam fluidized-bed dryer for parboiled rice: Testing of a pilot-scale and mathematical model development. *Drying Technol.* 24:1457–1467.

Stewart, O.J., Raghavan, G.S.V., Orsat, V., and Golden, K.D. 2003. The effect of drying on unsaturated fatty acids and trypsin inhibitor activity in soybean. *Process Biochem.* 39:483–489.

Svensson, C. 1980. Steam drying of pulp. In *Drying '80*, vol. 2, Ed. A.S. Mujumdar, pp. 301–307. New York: Hemisphere.

Taechapairoj, C., Dhuchakallaya, I., Soponronnarit, S., Wetchacama, S., and Prachayawarakorn, S. 2003. Superheated steam fluidised bed paddy drying. *J. Food Eng.* 58:67–73.

Taechapairoj, C., Prachayawarakorn, S., and Soponronnarit, S. 2004. Characteristics of rice dried in superheated steam fluidized-bed. *Drying Technol.* 22:719–743.

Tang, Z. and Cenkowski, S. 2000. Dehydration dynamics of potatoes in superheated steam and hot air. *Can. Agr. Eng.* 42:43–49.

Tang, Z., Cenkowski, S., and Izydorczyk, M. 2005. Thin-layer drying of spent grains in superheated steam. *J. Food Eng.* 67:457–465.

Uengkimbuan, N., Soponronnarit, S., Prachayawarakorn, S., and Nathkarankule, A. 2006. A comparative study of pork drying using superheated steam and hot air. *Drying Technol.* 24:1665–1672.

Wiriyaumpaiwong, S., Soponronnarit, S., and Prachayawarakorn, S. 2004. Comparative study of heating processes for full-fat soybeans. *J. Food Eng.* 65:371–382.

Yoshida, T. and Hyōdō, T. 1970. Evaporation of water in air, humid air, and superheated steam. *Ind. Eng. Chem. Process Des. Dev.* 9:207–214.